This is to certify that the

dissertation entitled

Deformation Structure of Spinodally Modulated

Cu-10Ni-6Sn Alloy

presented by

Shekhar Subramoney

has been accepted towards fulfillment
of the requirements for

Ph.D degree in Metallurgy

K. N. Subramanian
Major professor

Date 2/25/86.

DEFORMATION STRUCTURE OF SPINODALLY MODULATED

Cu-10Ni-6Sn ALLOY

By

Shekhar Subramoney

A THESIS

Submitted to
Michigan State University
in partial fulfillment of the requirements
for the degree of

DOCTOR OF PHILOSOPHY

Department of Metallurgy, Mechanics and Materials Science

1986

ABSTRACT

DEFORMATION STRUCTURE OF SPINODALLY MODULATED

Cu-10Ni-6Sn ALLOY

by

Shekhar Subramoney

The deformation structure in homogenized as well as spinodally modulated specimens of Cu-10Ni-6Sn alloy was investigated by transmission electron microscopy of thin foils prepared from bulk specimens deformed in uniaxial tension. Dislocations of predominantly edge character were observed along potentially operative slip traces of homogenized specimens. However, dislocations of random orientation were observed in specimens that had undergone the earlier stages of spinodal decomposition. Dislocations predominantly oriented at 60 degrees to their Burgers vector were observed in the slip traces of specimens that had undergone extensive aging.

Studies on the deformation characteristics of single crystal specimens oriented for single slip indicated that

increased extents of spinodal decomposition caused increasingly coarser slip. Percent elongation to fracture and work-hardening rate were not affected by the extent of composition modulation in this alloy.

ACKNOWLEDGEMENTS

The author would like to express his gratitude to Professor K. N. Subramanian for his guidance and support through the course of this investigation. Special thanks are also due to Professor N. Altiero and Professor C. M. Hwang of the Department of Metallurgy, Mechanics and Materials Science, and to Professor H. Eick of the Department of Chemistry for their helpful suggestions and encouragement.

The author would like to acknowledge the support of the U. S. Department of Energy through contracts DE-AC02-81ER10924 and DE-FG02-84ER45060. The extremely helpful and friendly suggestions provided by Professor Karen Baker and the staff at the Electron Optics Center are gratefully acknowledged. A special word of thanks is also due to Messrs. E. Ryan and A. Phillippedes of the HVEM facility at the Argonne National Laboratories. Thanks are also due to Professor P. Schroeder of the Department of Physics for help with the X-ray and spark-cutting units. Finally, the author would like to thank Dr. Tong-Chang Lee for being his best friend and an extremely generous research partner over the past four years.

TABLE OF CONTENTS

Page

LIST OF TABLES

LIST OF FIGURES

CHAPTER 1

INTRODUCTION

Phase transformations in alloys can be very broadly classified into two kinds. The first kind is the type of transformation that is large in degree but small in extent (namely, nucleation and growth of precipitates) and the second kind is the type of transformation that is small in degree but large in extent (namely, spinodal decomposition). Spinodal decomposition in alloys basically involves a periodic variation in space of local concentration of one of the alloying elements. This composition modulation is considered to be a sinusoidal variation in the earlier stages of spinodal decomposition, which can be expressed in terms of the following equation for cubic systems

$$c - c_0 = A(\cos 2\pi x/\lambda + \cos 2\pi y/\lambda + \cos 2\pi z/\lambda), \quad (1)$$

where, "c" is the local atomic concentration of the modulating element, "c_0" is the average atomic concentration of the modulating element, "A" is an amplitude factor of the modulation, and "λ" is the wavelength of the composition modulation. The x, y, and z axes referred to in Equation 1 are generally along the <100> directions for a cubic system.

The modulation caused by the decomposition during the aging of a spinodal alloy produces increases in the yield and flow stresses of the alloy, and this phenomenon is termed as age-hardening. Although several theories have been proposed to explain the age-hardening phenomenon, the actual mechanism is far from being understood.

1.1 Theory of Spinodal Decomposition

Although the spinodal phase has long been regarded as a limit beyond which a homogeneous phase is no longer metastable [1], it has become apparent that a phase beyond the spinodal phase would decompose by a simple diffusional clustering mechanism which is entirely different from the nucleation and growth mechanisms encountered for metastable phases. The theory of spinodal decomposition is based on the diffusion equation modified by thermodynamic requirements, and each parameter can be measured by independent diffusion or thermodynamic experiments.

In analyzing the characteristics of a spinodal alloy, the variation of the Helmholtz free energy "F" with composition at a constant temperature "T_0" is considered in a binary alloy system, as shown in Figure 1(a). The two inflection points "C_{s1}" and "C_{s2}" are defined by

$$(\partial^2 F/\partial C^2)_{T,V} = F'' = 0 , \tag{2}$$

where "C" is the atomic concentration of the second component, and "V" is the volume of the binary alloy. The points "C_{M1}" and "C_{M2}" are points of common tangency to the curve and they define the composition of the co-existing phases at "T_0". The locus of points satisfying Equation 2 for different temperatures is called the chemical spinodal and is shown by the dashed outer curve in Figure 1(b). The locus of points "C_{M1}" and "C_{M2}" for different temperatures is the solid curve in Figure 1(b) and it represents the miscibility gap. The significance of the spinodal curve is that alloys which become supersaturated by cooling from the homogeneous single phase solid solution region inside the miscibility gap will nucleate precipitates, whose distribution and morphology depend on whether the alloy is inside or outside the spinodal line. For alloys with compositions between the miscibility gap and the chemical spinodal line, F" is positive and there will be a nucleation barrier to precipitation, which means that the alloy will be stable with respect to small composition fluctuations. On the other hand, for alloys with compositions inside the spinodal line, F" is negative, there is, in principle, no

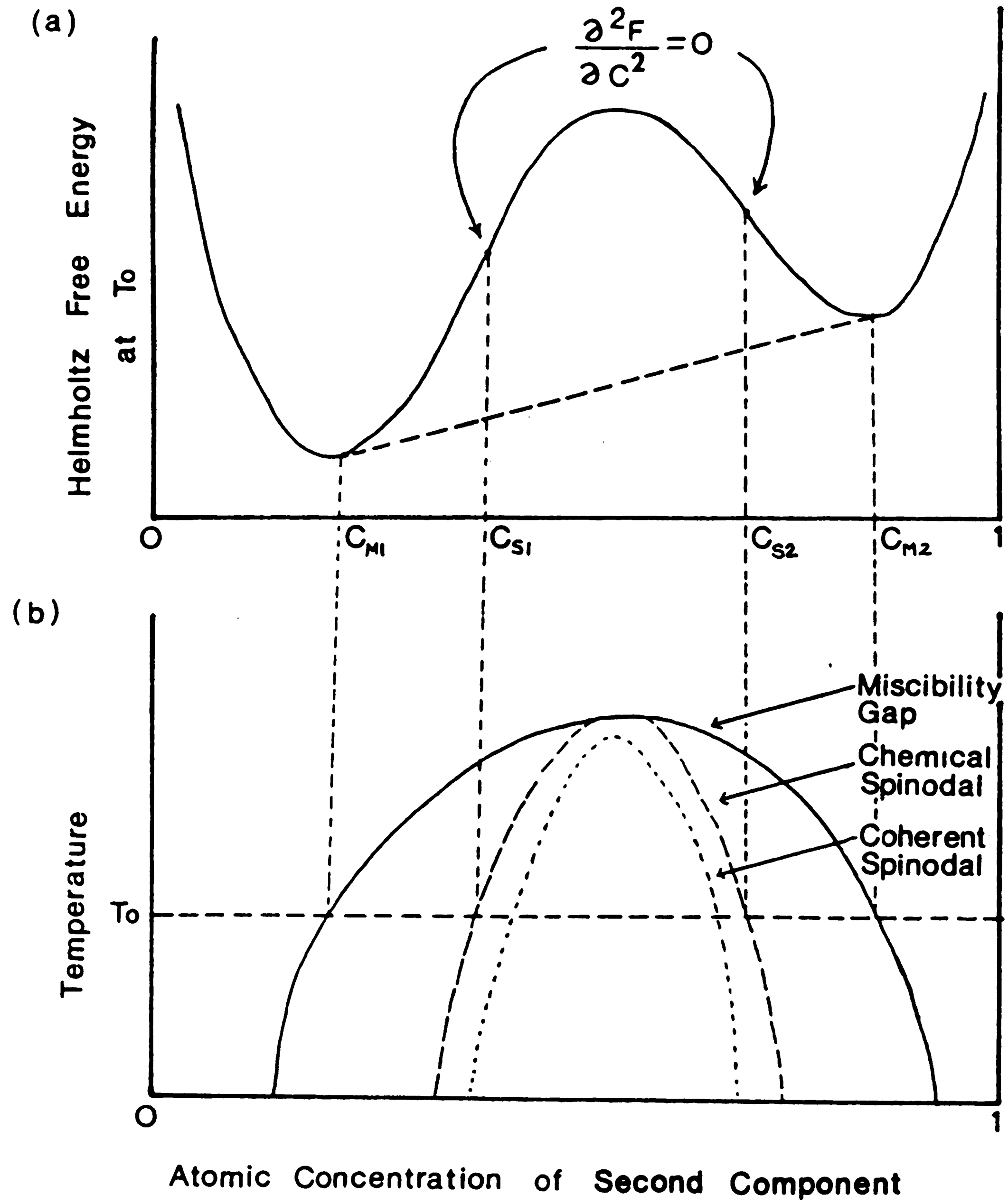

Figure 1: a) Schematic curve of the variation of Helmholtz free energy with composition at temperature T_0 for a binary alloy.

b) Phase diagram for the same system showing miscibility gap and the chemical and coherent spinodals.

nucleation barrier to precipitation and such an alloy is unstable to small composition fluctuations [2]. This implies that for such compositions, small compositional fluctuations result in decomposition into two phases denoted by "C_{H1}" and "C_{H2}" respectively.

Although spinodal decomposition was recognized by Gibbs [3], it is only recently that the theory of this kind of phase transformation has been developed by Hillert [4], and Cahn and Hilliard [5,6], to an extent where it can be used to predict microstructural aspects. It has been shown by these investigators that a solid solution inside the spinodal is unstable to sinusoidal fluctuations of wavelength "λ" when

$$\frac{\partial^2 f'(C)}{\partial C^2} + 2k\beta^2 + \frac{2\Omega^2 E}{(1 - \nu)} < 0, \qquad (3)$$

where "β" is the wavenumber = $2\pi/\lambda$, $f'(C)$ is the free energy of a unit volume of a homogeneous material of composition "C", "k" is a constant determined by the surface energy between the two phases, "E" is the Young's modulus, "ν" is the Poisson's ratio, and "Ω" is the linear dimensional variation of the lattice per unit composition change. The presence of a strain energy term in Equation 3 implies that the decomposition takes into account the elastic anisotropy of the crystal lattice. Since E is a minimum along the <100> directions in most cubic metals, three orthogonal compositional fluctuations along these directions are preferred. The microstructural result of this is a distribution of the second phase along the <100> directions, resulting in a three-dimensionally periodic distribution in space.

The first observation of spinodal decomposition was made in the early 1940's when Bradley [7] observed sidebands around the sharp Bragg spots of the diffraction pattern from a Cu-Ni-Fe alloy that had been quenched and annealed in the region of the miscibility gap. Daniel and Lipson [8,9], studying the same system, explained this phenomenon as a periodic modulation of composition along the <100> directions, and they were also able to measure the wavelength of this modulation.

In order to account for the effect of the coherency strains, Cahn [6] introduced an additional term in Equation 2, and modified it to

$$F'' + 2\eta^2 Y = 0, \tag{4}$$

where "Y", for the case of <100> modulations, can be expressed in terms of the elastic constants "C_{ij}" as

$$Y = \frac{(C_{11} - C_{12})(C_{11} + 2C_{12})}{C_{11}} . \tag{5}$$

The locus of points satisfying Equation 4, which always lies inside the chemical spinodal, is defined as the coherent spinodal, and is shown in Figure 1(b).

1.2 Theoretical Models on the Age-Hardening Mechanism of Spinodal Alloys

The role of long range coherent composition fluctuations resulting from spinodal decomposition on mechanical properties of cubic crystals has been the subject of extensive investigations. One of the first theoretical models to explain the age-hardening mechanism in spinodal alloys was developed by Cahn [10], who considered a dislocation lying on the (111) slip plane of a face-centered cubic alloy. The stress field due to the composition modulation on this slip plane is given as

$$\tilde{\sigma} = \begin{pmatrix} S_2(y)+S_3(z) & 0 & 0 \\ 0 & S_1(x)+S_3(z) & 0 \\ 0 & 0 & S_1(x)+S_2(y) \end{pmatrix} .$$

where,

$$S_1(x) = A\Omega Y\cos(\beta x), \tag{6}$$

$$S_2(y) = A\Omega Y\cos(\beta y), \text{ and} \tag{7}$$

$$S_3(z) = A\Omega Y\cos(\beta z). \tag{8}$$

The equation of this slip plane can be considered as

$$x + y + z = \sqrt{3}d, \tag{9}$$

where "d" is the interplanar distance for the (111) kind of lattice planes. Rotating the co-ordinate system to x y z such that x' lies along $[1\bar{1}0]$, y' along $[11\bar{2}]$ and z' along [111], the resolved force on a dislocation lying along [110] due to the internal stress field can be written as

$$\vec{b}.\tilde{\sigma}.\hat{n} = \frac{\sqrt{2}}{\sqrt{3}}\left[A\Omega Yb \sin\left(\frac{\beta x'}{\sqrt{2}}\right) \sin\left(\frac{\beta y'}{\sqrt{6}}\right)\right], \tag{10}$$

where "$\vec{b}$" is the Burgers vector and "$\hat{n}$" is the unit normal to the glide plane. The stress field on the (111) slip plane can be represented as a rectangular checkerboard of alternating regions, as shown in Figure 2. The sides of these rectangles are the locus of zero stress positions and within each rectangle the stress rises or falls to an extremum in the center.

The other forces on the dislocations are due to the curvature of the dislocation (or its self stress), and due

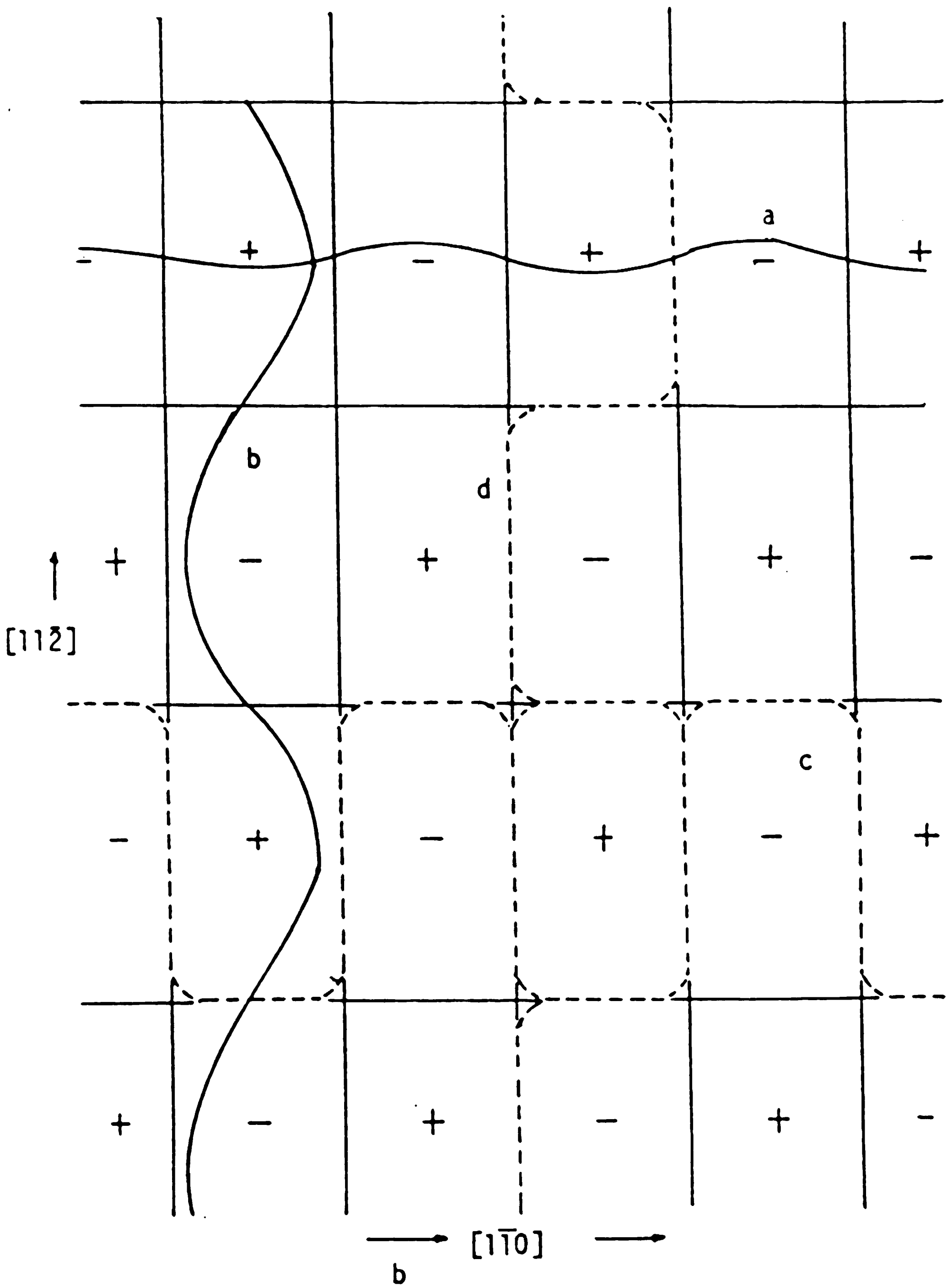

Figure 2: The (111)[1$\bar{1}$0] slip system in the absence of applied stress showing the forces on the dislocations and the resulting configurations [10],

a) screw,

b) edge.

to the external applied stress. Under equilibrium, the sum of all the forces on a dislocation due to the self stress of the dislocation, the internal stress field caused by the modulation and the external applied stress is equal to zero. This force-balance equation is known as the Peach-Koehler equation, and can be written as

$$\frac{\Gamma(\frac{d^2y'}{dx'^2})}{[\ 1\ +\ (\frac{dy'}{dx'})^2\ ]^{3/2}} + \frac{\sqrt{2}}{\sqrt{3}}\ A\eta Yb\ \sin(\frac{\beta x'}{\sqrt{2}})\ \sin(\frac{\beta y'}{\sqrt{6}})\ +\ |\sigma|b\ =\ 0, \qquad (11)$$

where "Γ" is the line-tension of the dislocation, and "σ" is the external applied stress.

In order to solve this non-linear equation, Cahn [10] assumed the following solutions.

$$y' = C_1\ +\ C_2 \sin(\frac{\beta x'}{\sqrt{2}}), \qquad (12)$$

and

$$x' = B_1\ +\ B_2 \sin(\frac{\beta y'}{\sqrt{6}}), \qquad (13)$$

for screw and edge dislocations respectively. C_1, C_2, B_1 and B_2 are constants. Using the Galerkin method along with the assumptions that βB_2 and βC_2 are very much less than unity, Cahn [10] arrived at the following solutions. In the

case of screw dislocations

$$C_2{}^2 = \frac{4\ A^2 \Omega^2 Y^2 b^2}{3\ \beta^4 \Gamma^2}\left(1 \pm \sqrt{1 - \frac{54\sigma^2 \beta^2 \Gamma^2}{A^4 \Omega^4 Y^4 b^2}}\right), \tag{14}$$

and in the case of edge dislocations

$$B_2{}^2 = \frac{12\ A^2 \Omega^2 Y^2 b^2}{\beta^4 \Gamma^2}\left(1 \pm \sqrt{1 - \frac{\sigma^2 \Gamma^2 \beta^2}{A^4 \Omega^4 Y^4 b^2}}\right). \tag{15}$$

It can be seen that there is no stable solution when $(1 - 54\sigma^2 \beta^2 \Gamma^2 / A^4 \Omega^4 Y^4 b^2)$ and $(1 - 2\sigma^2 \beta^2 \Gamma^2 / A^4 \Omega^4 Y^4 b^2)$ are negative. In order to determine the critical resolved shear stress, it is necessary to determine the maximum value of "σ" as imposed by the conditions given above.

This provides the following values

$$\sigma_s = \frac{A^2 \Omega^2 Y^2 b}{3\sqrt{6}\beta\Gamma}, \tag{16}$$

for screw dislocations, and

$$\sigma_E = \frac{A^2 \Omega^2 Y^2 b}{\sqrt{2}\ \beta\Gamma}, \tag{17}$$

for edge dislocations.

Since $\sigma_s < \sigma_E$, Cahn theorized that screw dislocations, which are set in motion at a lower value of critical resolved shear stress, are responsible for the age-hardening in spinodal alloys. But the major drawback of Cahn's theory is that experimentally obtained values of yield stress for spinodally modulated structures are very much higher than theoretically predicted values, as noted by Douglass and Barbee [11], Ditchek and Schwartz [12] and Lefevre, D'Annessa and Kalish [13]. Moreover, the predicted A dependence of the yield stress has not been found to be true by Butler and Thomas [14] and Lefevre et al [13].

The effect of lattice mismatch was considered to explain the age-hardening mechanism in spinodal systems by Carpenter [15] and Ditchek and Schwartz [16]. For example, in the experimental work on 60Au-40Pt alloys, Carpenter [15] has considered the alloy lattice to be a sequence of alternating gold and platinum-rich regions along the <100> directions, where the lattice mismatch shearing strains are caused by shearing a Pt-rich region over a Au-rich region and vice-versa. Similar to Cahn's [10] theory, the yield stress is proportional to $A^2\lambda$ in Carpenter's [15] theory. According to this model

$$\sigma_s = \frac{(A\eta)^2 E^2 \lambda}{2\pi\sqrt{6}Gb}, \qquad (18)$$

and

$$\sigma_s = \frac{(A\Omega)^2 E^2 \lambda}{2\pi\sqrt{2}Gb} \quad . \tag{19}$$

The important role of dislocation self-stress is neglected in the theories of Carpenter [15] and Ditchek and Schwartz [16]. As a result these models cannot be considered to be complete.

Ghista and Nix [17] developed a model where it was assumed that there is a variation in the elastic energy of a dislocation in an inhomogeneous material. Since this theory is based on the elastic interaction between dislocations and periodic fluctuations of the shear modulus, it was assumed that the variation in the shear modulus can be represented by a first kind Bessel function of order either 0 or 1. This model suggests that the critical stress to initiate plastic flow increases linearly with the amplitude of the shear modulus variation, and varies inversely with the wavelength, and can be represented by

$$\sigma = \left(\frac{P}{E}\right)_{max} \bar{G}b \left(\frac{1.75x10^{-3}}{\lambda} \right) , \tag{20}$$

where "$\bar{G}$" is the average shear modulus, $\bar{E} = \bar{G}b^2$, and "P" is the force intensity on a dislocation. The major drawbacks

in their theory are the consideration of a straight dislocation and the neglect of the contribution by the internal coherency stress. They also did not consider the self energy of the dislocation to be a completely periodic function of its position.

The theory of Dahlgren [18] considers the yield stress to be dependent only on the differences in cubic lattice parameters of unstressed precipitating phases or internal coherency stresses, and is independent of other factors such as the precipitate particle size and volume fractions. He obtained the yield strength of age-hardened spinodal alloys as

$$\sigma = Y\Delta a/3\sqrt{6}a_0, \tag{21}$$

where "Δa" and "a_0" are the difference in and the average cubic lattice parameter of the precipitating phase. This theory is not complete as it assumes a straight dislocation and neglects the effect of dislocation self stress.

The evaluation of interfacial energy per unit area of slip plane was considered by Hanai, Miyazaki and Mori [19] to explain the age-hardening mechanism in spinodal alloys. They proposed that new interfaces are created on a slip plane when a crystal with continuous composition fluctuations due to spinodal decomposition is deformed by slip, and the energy of such interfaces was evaluated on that basis. Hanai et al. concluded that the contribution of the interfacial energy was large enough to account for the age-hardening, and their calculations for a face-centered cubic structure give

$$\sigma = (4\sqrt{2}\pi/9)(2U_{E} n_{c} n_{s} + sG\eta^{2})A^{2}\lambda^{-1}, \text{ and} \tag{22}$$

$$\sigma = (\sqrt{6}\pi/3)(2U_{E} n_{c} n_{s} + sG\eta^{2})A^{2}\lambda^{-1} \tag{23}$$

for screw and edge dislocations respectively, where "U_E" is the interchange energy of atom pairs, "n_c" is the co-ordination number, "n_s" is the number of atoms per unit area of the interface and "s" is a constant related to the shape of the solute rich region.

The major drawback in the theory of Hanai et al. is the consideration of the interfacial energy to be the sum of the chemical interfacial energy, which is defined per unit area, and the elastic strain energy, which is defined per unit volume. Also, the assignment of interfacial energy to be 0.3 J/m^2 is an overestimation, since the modulated structure in spinodal alloys is characterized by the fluctuation of constitutive atoms and is not brought about by an entirely different atomic arrangement as envisaged in a grain or twin boundary.

The theory of Kato, Mori and Schwartz [20] uses the same approach as that of Cahn [10]. They also considered the Peach-Koehler force-balance equation, but considered a mixed dislocation lying mainly in the positive regions of the internal stress field as shown in Figure 3 to be responsible for the macroscopic yielding. Using similar assumptions, and with an appropriate rotation of the co-ordinate system with respect to that used by Cahn [10], Kato et al. [20] evaluated that

$$C_2{}^2 = \frac{6A\eta Yb\Gamma\beta \pm 4A\eta Yb^2\sqrt{A^2\eta^2Y^2 - 6\sigma^2}}{(24\sigma^2b^2 + 9\Gamma^2\beta^2 - 4A^2\eta^2Y^2b^2)\ \beta}, \tag{24}$$

for a mixed dislocation which is oriented at 60 degrees to the Burgers vector. There is no stable dislocation configuration when $(A^2\eta^2Y^2 - 6\sigma^2)$ is negative and the critical resolved shear stress using the mixed dislocation model is given by

$$\sigma_M = A\eta Y/\sqrt{6}. \tag{25}$$

According to this model, the critical resolved shear stress is independent of "λ". The theory of Kato et al. therefore argues that screw and edge dislocations will move at lower stresses as predicted by Cahn [10] causing microyielding. Inhibited by pinning due to the modulated structure, these

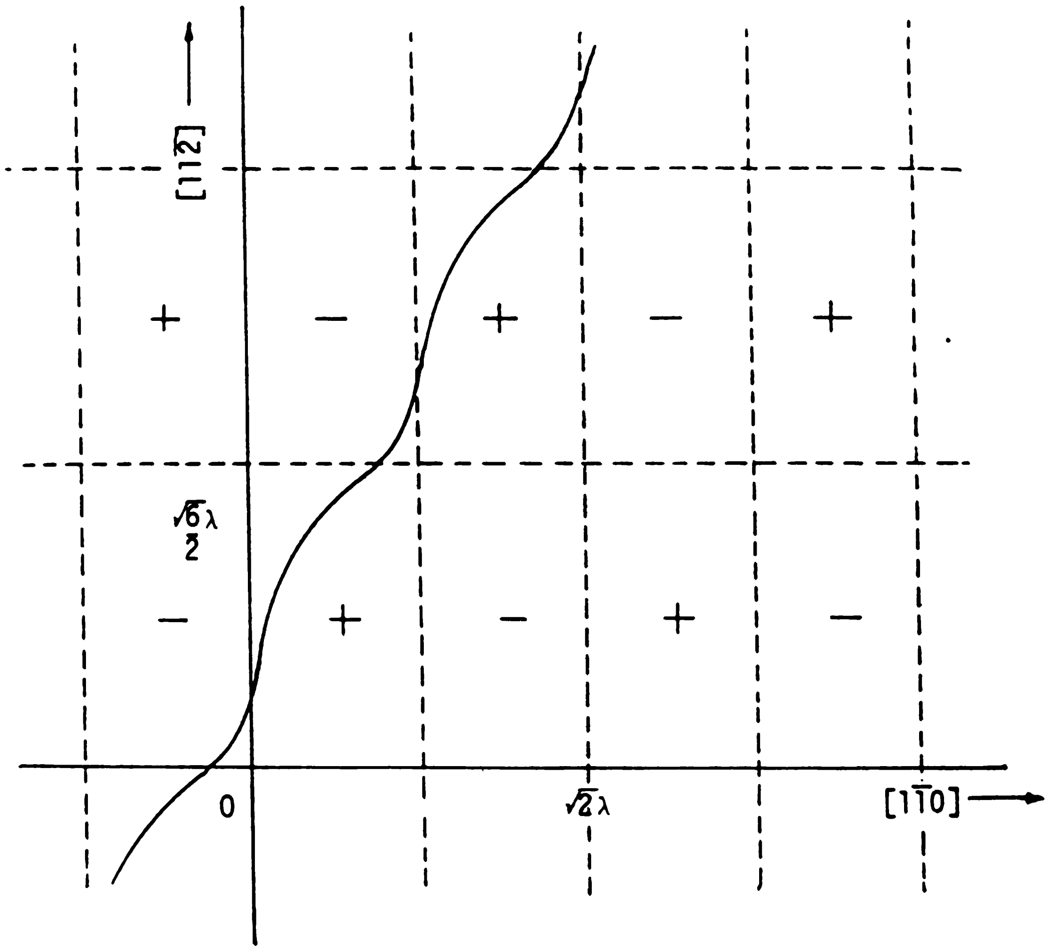

Figure 3: Schematic representation of a mixed dislocation and internal stress profile considered by Kato, Mori and Schwartz [20].

dislocations will reorient into the mixed configuration which suffers the largest resistance to motion of all possible orientations. Kato et al. suggest that the motion of these dislocations with mixed character to be responsible for the macroyielding.

A review article by Wagner [21] on the various theories of hardening by spinodal decomposition has suggested that of all the theories, only those proposed by Cahn [10] and Kato et al. [20] have any validity in explaining the age-hardening during early stages of spinodal decomposition. Recently, Ardell [22] has criticized both of these theories on the basis that they predict the critical resolved shear stress of an ideal microstructure. He sought to explain the age-hardening phenomenon of spinodal alloys by considering a microstructure which is modulated but not perfectly periodic. His theory is therefore based on hardening by strong diffuse obstacles and considers the statistical aspects of the microstructure. Ardell's theory is similar to that of Cahn [10] and Kato et al. [20] in that the critical resolved shear stress is the stress required to liberate the dislocation from the obstacles trapping it.

The interaction between dislocations and strong diffuse obstacles was initially considered by Mott [23]. He derived the following equation for the critical resolved shear stress under such conditions;

$$\sigma = \frac{2\Gamma w^{1/3} \beta_c^{4/3}}{b\ L_s^{4/3}} , \tag{26}$$

where "w" is the range of interaction between an obstacle and a dislocation, "β_c" is the dimensionless critical force exerted by a dislocation on an obstacle and "L_s" is the square lattice spacing.

In order to apply Equation 26 to the problem of spinodal decomposition, Ardell [22] considered $L_s \approx \lambda$ (as per the theory of Nabarro [24]) and obtained "β_c" and "w" from the solutions of Cahn [10] for the periodic shape of the edge dislocation, where

$$\beta_c = \frac{A\eta Y b\lambda}{\sqrt{2}\pi\Gamma} , \quad \text{and} \tag{27}$$

$$w = \frac{\sqrt{3}A\eta Y b\lambda^2}{2\pi^2\Gamma} . \tag{28}$$

Since the experimentally obtained values of critical resolved shear stress for the Cu-Ni-Fe spinodal systems match very closely with those calculated with edge dislocations in his model, Ardell attributes the hardening to dislocations of this specific character. Ardell [22] proposed that the interaction of edge dislocations with strong diffuse obstacles in a non-ideal microstructure is responsible for the age-hardening in spinodal alloys. His

equation is obtained by making substitutions for "L_s", "β_c" and "w" into Equation 26 and is given by

$$\sigma = 0.122(A\eta Y)^{3/2}(\lambda b/\Gamma)^{1/2} \quad . \tag{29}$$

The numerical co-efficient in Equation 29 depends on the dislocation character. It is 0.041, 0.122 or 0.026 for screw, edge or mixed dislocations at 60 degrees to their Burgers vector respectively. Since "Γ" is smallest for edges, "σ" is significantly larger for edge dislocations as compared to screw or mixed dislocations.

1.3 Experimental Investigations on Spinodal Alloys

Experimental studies on the various mechanical properties of spinodal alloys have been carried out by a number of investigators [11, 14, 15, 25-45]. Transmission electron microscopy has been used extensively to visualize the spinodal microstructure, to measure the wavelength and waveshape and to analyze dislocations present in deformation structure. Schwartz, Mahajan and Plewes [25] investigated the microstructural features of homogenized and aged Cu-9Ni-6Sn alloy. The principal feature observed by them was the appearance of modulated regions which appeared to exhibit some order in their arrangement along the <100> directions. Similar structural features were observed by Livak and Thomas [26] and Butler and Thomas [14] in Cu-Ni-Fe

alloys, and by Laughlin [27], in Ni-Ti alloys which also decompose spinodally. Butler and Thomas [14] determined the modulation wavelength from the sidebands in electron diffraction patterns and the modulation amplitude from magnetic Curie point measurements. Ditchek and Schwartz [28] measured the modulation parameters in Cu-10Ni-6Sn by x-ray diffraction methods.

Later stages of spinodal decomposition causes intergranular precipitates which significantly decrease the ductility of the alloys. The precipitation reaction at the later stages of decomposition was investigated by Carpenter [15] in Au-Pt alloys, by Douglass and Barbee [11] in Al-Zn alloys, by Schwartz et al. [25] and Ditchek and Schwartz [28] in Cu-Ni-Sn alloys, and by Wu and Thomas [29] in Cu-Ni-Cr alloys.

The results obtained by Butler and Thomas [14] on Cu-Ni-Fe alloys indicated that the incremental yield stress due to spinodal decomposition is dependent only on the modulation amplitude. The same conclusion was drawn by Dahlgren [30] who studied Cu-Ni-Fe alloys as well. The dependence of incremental yield stress on the variation of lattice parameter was determined by Wu and Thomas [29] in their work on Cu-Ni-Cr alloys. Chou and coworkers [31] have pointed out that the interaction of dislocations with the periodic internal stress field produced by spinodal

decomposition of Cu-Ni-Cr alloys is responsible for the age-hardening. Similar observations were made by Datta and Soffa [32] on Cu-Ti alloys. A number of other investigators have examined the age-hardening mechanism in Cu-Ti alloys [33, 34].

The flow and fracture behavior of Cu-Ti single crystal specimens was studied by Greggi and Soffa [35]. They found that the critical resolved shear stress increased with aging time but the total strain decreased with aging time, presumably due to coherent precipitates. The properties of Cu-Ti single crystals have also been studied by Kratochvil and Haasen [36].

The mechanical properties of the Cu-10Ni-6Sn spinodal alloy have been investigated extensively [37-44]. Kato and Schwartz [37] have determined that the incremental yield stress is independent of the test temperature, and that the activation volume and work-hardening rate are independent of the extent of decomposition. The total elongation is also independent of the extent of decomposition, as determined by Vilassakdanont and Subramanian [38]. Similar results have been obtained by Lee et al. [39] and by Shekhar et al. [40]. Quin and Schwartz [41, 42] have found that the fatigue properties are not improved by spinodal decomposition in Cu-10Ni-6Sn. They attributed this to the local demodulation

caused by the to-and-fro motion of dislocations which leads to a cyclic softening of the material. Similar results were obtained in Cu-Ti alloys by Sinning and Haasen [45].

In this investigation the nature of dislocations in aged and deformed specimens of Cu-10Ni-6Sn in which the uniaxial tensile direction was carefully identified was studied to gain a better understanding of the mechanism of age-hardening in spinodally modulated structures. The results were correlated to those obtained from <u>in-situ</u> deformation experiments of similar specimens in the High Voltage Electron Microscope [46]. The deformation characteristics of single crystal specimens oriented for single slip were also studied to gain a better understanding of the mechanism.

CHAPTER 2

EXPERIMENTAL PROCEDURE

2.1 Specimen Preparation

The Cu-10 wt.%Ni-6wt.%Sn alloy used in the present study was prepared at the Bell Laboratories. The choice was made on the basis of its cubic structure, the relative ease in controlling at desired stages of decomposition as well as on the basis of the availability of experimental data for mechanical properties of bulk specimens [12, 25, 26, 37, 44]. The procedure used for preparing this alloy is described in a paper by Schwartz, Mahajan and Plewes [25].

The as-received stock was rolled down to a thickness of about 0.5 mm using a standard cold-rolling mill. Rectangular strips 40mm x 7mm were cut out from the rolled-down sheet. These strips were solution-treated at 1073 K for three minutes in argon atmosphere in a tube furnace in order to remove all residual stresses due to

prior mechanical working, and quenched in cold water to prevent any spinodal decomposition. Since large grain size is beneficial to dislocation analysis by transmission electron microscopy, grain growth was achieved by using a strain-annealing method. This was carried out by imparting a critical plastic strain of 8% to the specimens followed by annealing at 1073 K for 72 hours in vacuum in the tube furnace followed by quenching in cold water. This procedure produced specimens with grain sizes of 0.5 to 1 mm diameter. Specimens that did not receive any further heat treatment are referred to as "homogenized specimens" in this thesis. Some of the as-quenched specimens were aged at 623 K for 5, 20, 40 and 60 minutes in order to induce varying extents of composition modulation due to spinodal decomposition followed by quenching in water. These specimens are referred to as "aged specimens" in this thesis. The flow chart for specimen preparation is shown in Figure 4.

The homogenized and aged specimens were deformed to about 5% plastic strain by uniaxial tension using a micro-tensile fixture in an Instron tensile testing machine. The micro tensile fixture and the manner in which it is fitted in the tensile testing machine are shown in Figures 5 and 6 respectively. In order to prepare the deformed specimens for transmission electron microscopy, the strips were chemically thinned down to 100 μm using a solution of 40% nitric acid and 60% distilled water at room temperature.

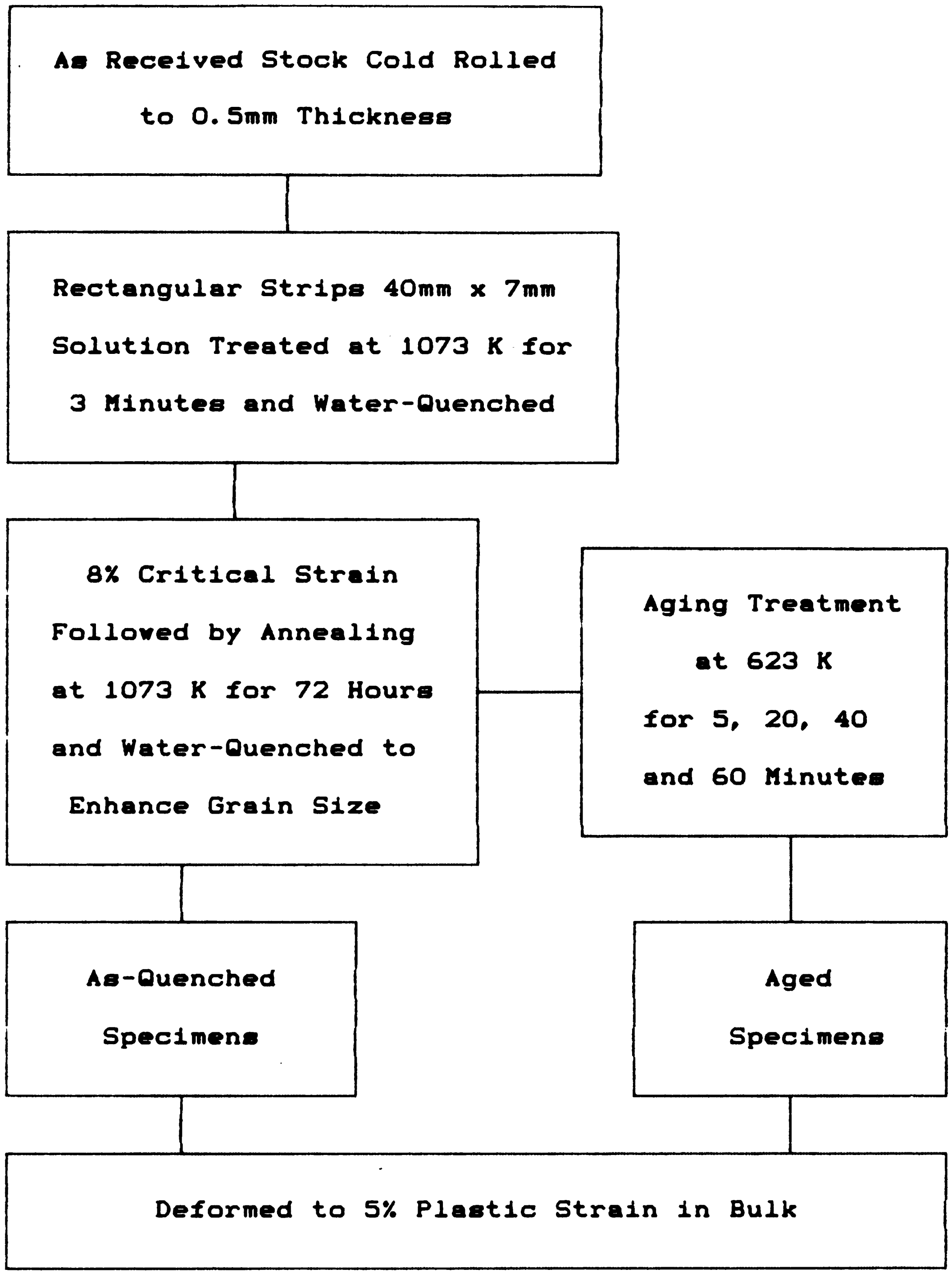

Figure 4 Flow chart showing steps used for the grain growth and aging treatments of the Cu-10Ni-6Sn alloy.

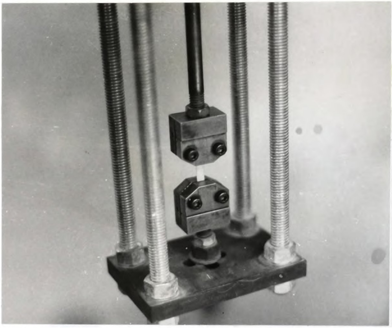

(a)

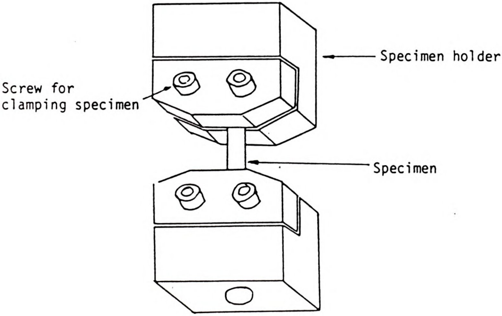

(b)

Figure 5: Microtensile fixture used in Instron testing machine;

a) photograph,

b) schematic.

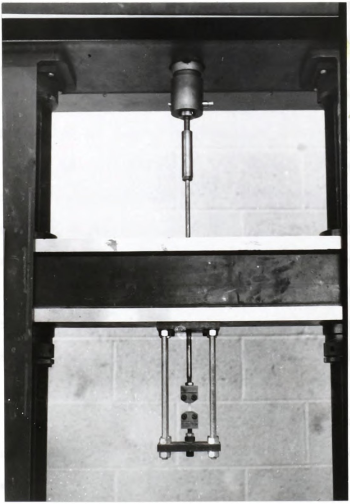

Figure 6: Photograph of the microtensile fixture as mounted on the Instron testing machine.

The direction of uniaxial tension was marked on the thinned down strips and disks 3mm in diameter were cut out in such a way that this line was identified on the disks. The central portion of the disks was made transparent to the electron beam by using a two-step electropolishing method. The first step involved single jet electropolishing, and Figure 7 shows the set-up used for this step. The specimen was placed in the center of the platinum wire coil and electropolished under a jet stream of electrolyte for about 15 seconds in order to produce a polished concave surface. The electropolishing solution and the conditions used for electropolishing in this step are shown in Table 1. The specimen was then turned over and the jet polishing was resumed on the other side of the specimen for the same length of time. The jet polished specimens were washed in methanol, dried and stored for final electropolishing.

In the second step, the specimen was electropolished to produce the perforation in the center of the disk. The electrolyte and temperature conditions are the same as that for the first step, however, the electropolishing voltage and current conditions are different, as indicated in Table 2. The set-up used in this step is shown in Figure 8. The specimen was held between two platinum loops attached to the tips of a reverse-action tweezer, which is shown in Figure 9. The cathode was a cylindrical stainless sheet with slots cut out. A pointed light source was used to determine when

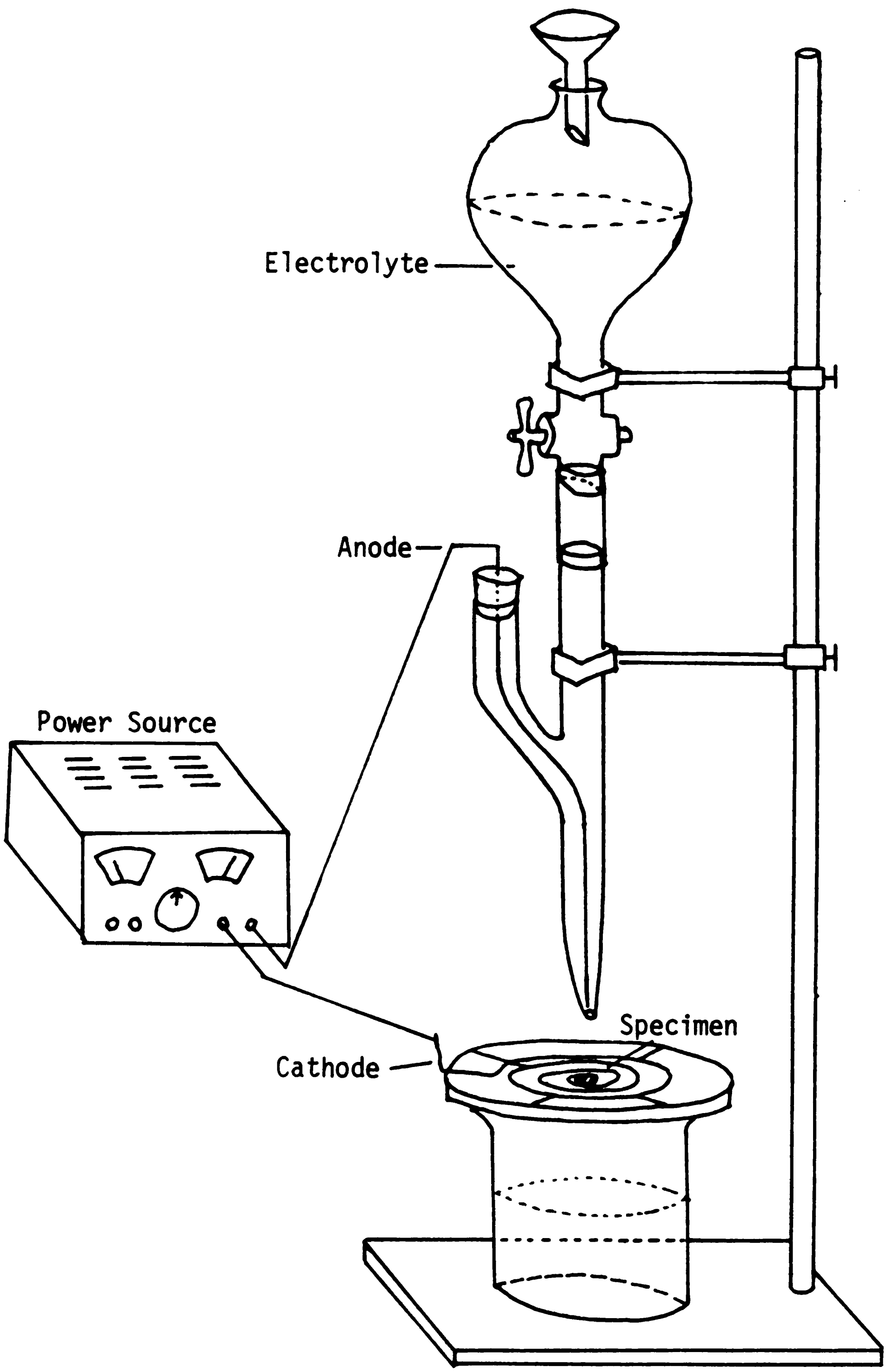

Figure 7: Schematic of the single-jet electropolishing unit.

Table 1 Data for Single-Jet Electropolishing.

Composition of Electrolyte	Voltage (V)	Temperature (K)
80% Methyl Alcohol 20% Nitric Acid	50	273

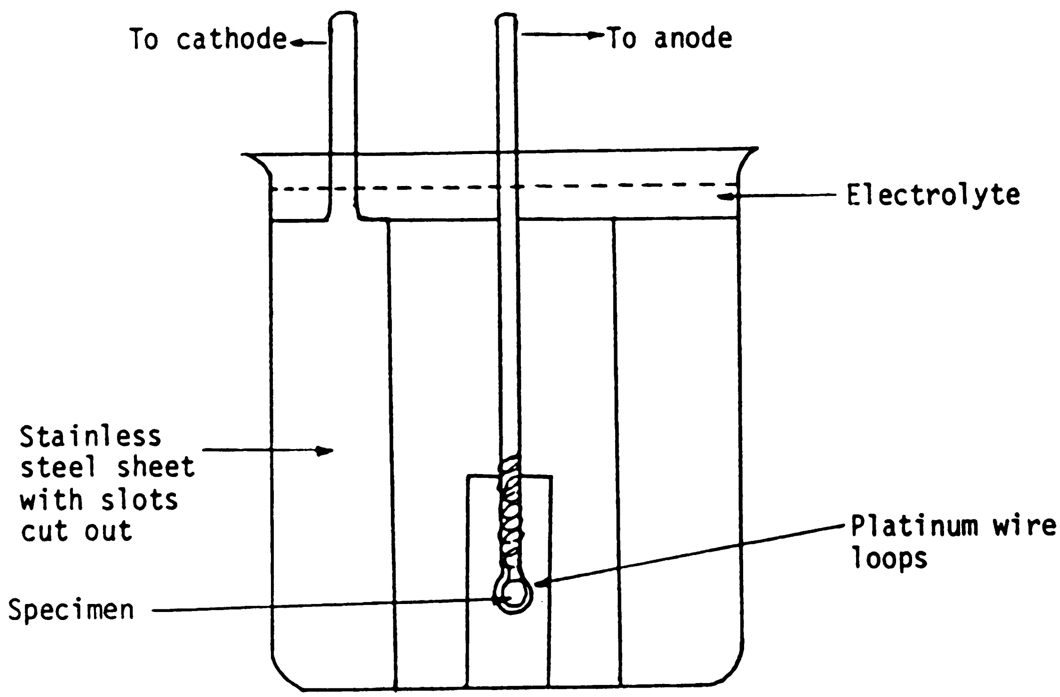

Figure 8: Schematic of the final electropolishing unit.

Table 2 Electropolishing Data for Final Step of Thin Foil Preparation.

Composition of Electrolyte	Voltage (V)	Temperature (K)
80% Methyl Alcohol 20% Nitric Acid	8	233

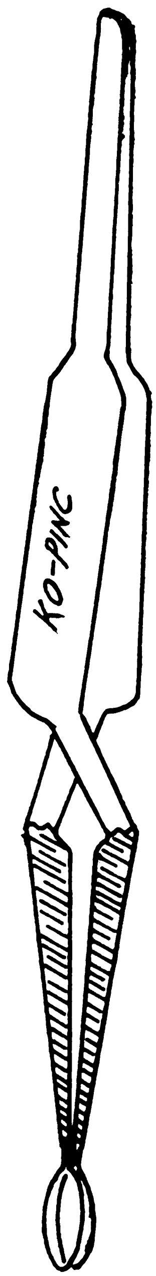

Figure 9: Specimen holder for final electropolishing consisting of platinum loops attached to the tips of a reverse action tweezer.

perforation occurred in the center of the disk, and as soon as this took place, the specimen was removed from the electrolyte and washed thoroughly in running methanol. The final electropolishing step was always carried out just before the insertion of the specimen into the transmission electron microscope (TEM), in order to minimize any oxidation or contamination problems.

2.2 Transmission Electron Microscopy

The transmission electron microscope used in the study of dislocations present in slip traces of deformed specimens was the Phillips EM 300 equipped with a goniometer stage. The TEM was operated at 100 kilovolts. The specimen holder was capable of single tilt to the extent of +45 degrees. The specimen was mounted in such a way that the original tensile direction (already identified on the disk) was always along the axial direction of the specimen holder. Since the image rotation with respect to the object in the electron microscope was already determined for given operating conditions, it was easy to identify the direction of the tensile axis in the image within reasonable accuracy. Once a set of dislocations lying along a slip trace was observed in the image, the Schmidt factor was determined for the slip system concerned, and this was used as a guideline to determine whether the slip system was potentially operative during tensile deformation of the bulk specimen.

The Burgers vector of dislocations present in slip traces that could have been operative during bulk deformation was identified by the "two-beam condition" method. This was performed by obtaining a number of images of the same field of view using different diffracting planes. An ideal two-beam condition is obtained when one of the diffracted spots in the electron diffraction pattern is as bright as the transmitted or (000) spot, while the rest of the spots are nearly invisible. This is achieved by tilting the specimen so that the incident beam direction is close to one of the major zone axes. A series of different two beam conditions can be obtained by tilting the specimen through a small angle (of the order of 5 to 10 degrees) about a series of different axes in the diffraction pattern. The diffraction vectors $\vec{g}$ normal to the diffracting planes were determined from these two-beam conditions; $\vec{g}$ is also the vector connecting the bright diffracted spot to the transmitted spot on the diffraction pattern.

When a series of bright field images with their corresponding two-beam condition diffraction patterns was recorded, the "$\vec{g}.\vec{b} = 0$" criterion was applied to determine the direction of the Burgers vector. Dislocations are out of contrast when $\vec{b}$ is lying on the diffracting plane, and two conditions where the dislocations are out of contrast imply that $\vec{b}$ is common to both diffracting planes and is the

zone axis of the two diffracting planes.

Trace analysis using stereographic projections was used to identify the dislocation line direction. Possible slip planes were identified from the fact that the Burgers vector of the dislocations concerned is always lying on its slip plane. Using the great circles representing these slip planes in the stereographic projection, the dislocation line direction was determined. This can be carried out since the image of the dislocation on the micrograph represents the projection of the dislocation onto the plane of the micrograph. The true dislocation direction is parallel to the projected direction and passes through the center of the stereographic projection. The character of the dislocations in the concerned slip traces was determined by using their Burgers vectors and dislocation line directions.

2.3 Single Crystal Specimens

The single crystal of Cu-Ni-Sn was grown using the Czochralski method in which the melt was held in a graphite crucible at a temperature of 1370 K. The seed used was a single crystal of pure copper, and the crystal growth direction was close to [100]. The crystal thus obtained had approximate dimensions of 6 cm x 1 cm x 1 cm. It was verified that the entire specimen was a single crystal by

obtaining Laue x-ray back-reflection patterns at various points along the length and width of the specimen. A special goniometer stage, which can rotate about all three axes, and which can be mounted on the x-ray machine as well as on the spark cutting machine, was used to hold the specimen. A photograph of this goniometer stage is shown in Figure 10. In order to obtain specimens which would deform by single slip, it was necessary to orient the single crystal along a tensile direction that would have a Schmidt factor as close to 0.5 as possible. The orientation was achieved with the aid of Laue x-ray back reflection patterns. Figure 11 is a stereographic projection corresponding to the Laue back reflection pattern obtained when the single crystal was oriented along the tensile direction suitable for single slip. Analysis of this pattern indicated that this direction was very close to $[\bar{1}45]$, which provides a Schmidt factor of 0.47 on the potential slip system. The corresponding slip plane and slip direction are shown in Figure 12. Once the specimen was thus oriented, it was cut into tensile samples of approximate dimensions 10 mm x 2 mm x 2 mm in a wire spark cutter, which is shown in Figure 13.

The single crystal specimens obtained from the spark cutting machine had serrated surfaces, which were smoothed down using a very fine 600 grit emery paper. The specimens were chemically polished in a solution containing 40% nitric

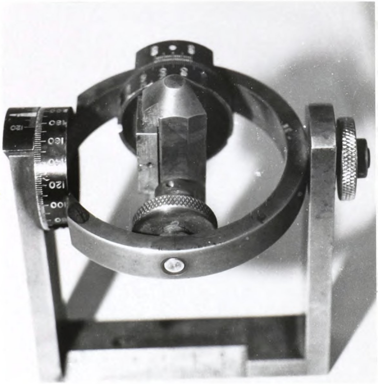

Figure 10: Goniometer stage used in x-ray diffraction analysis and spark cutting of single crystal specimens.

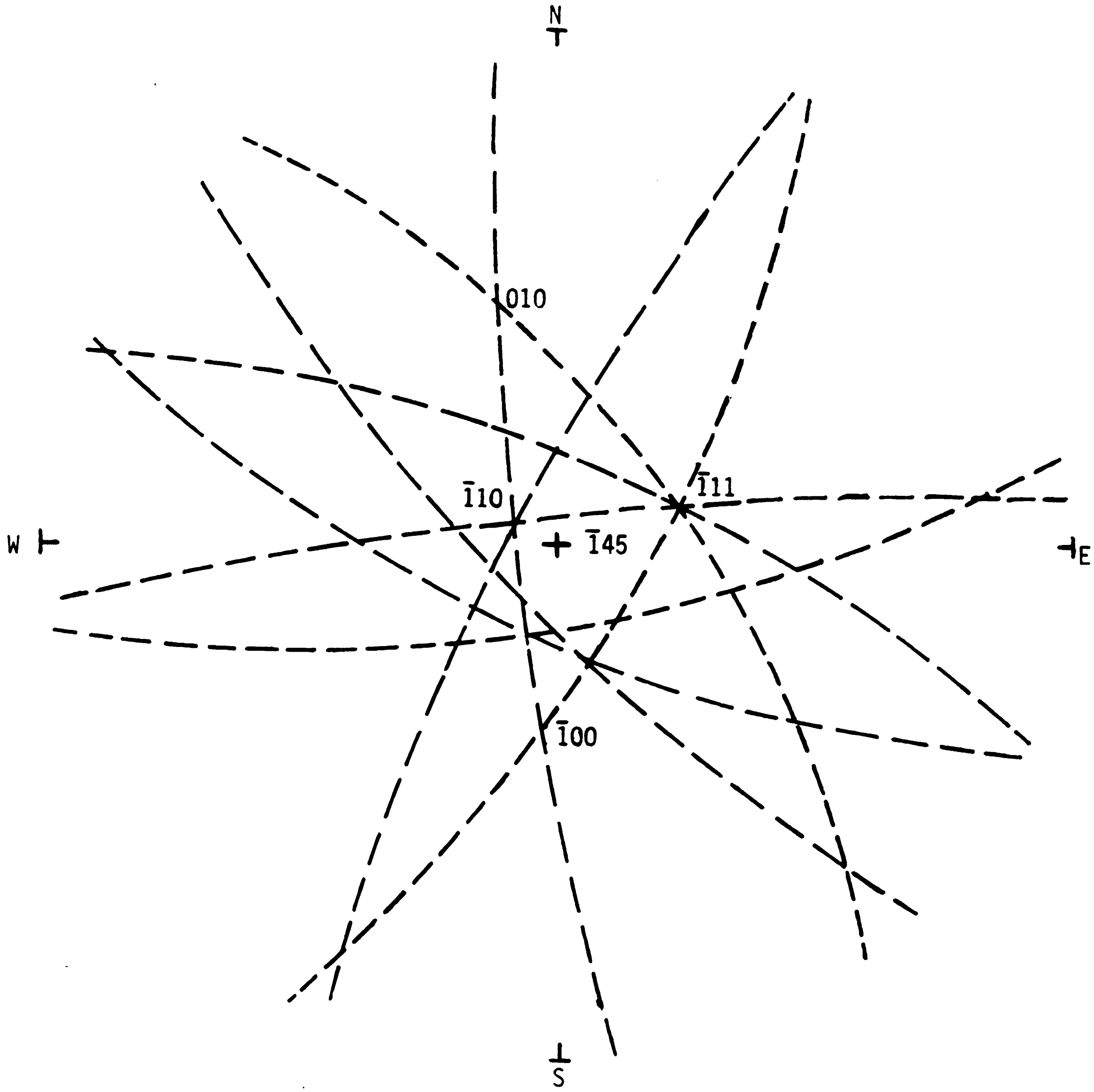

Figure 11: Stereographic projection corresponding to the Laue x-ray back reflection pattern of single crystal specimen oriented for single slip.

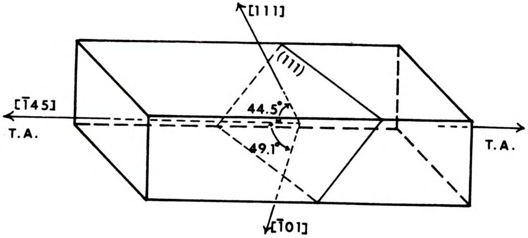

Figure 12: Schematic of single crystal specimens illustrating tensile direction and potential single slip system.

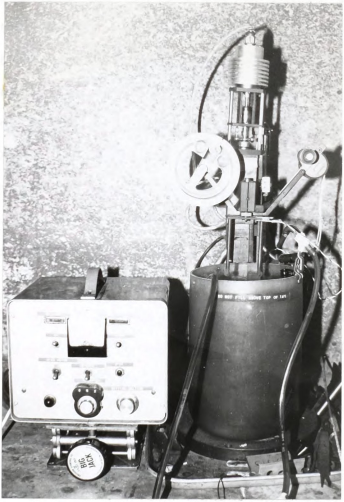

Figure 13: Photograph of the wire spark cutting machine used in slicing the single crystal specimens.

acid and 60% distilled water to obtain smooth surfaces. Solution treatment was carried out at 1073 K for two hours in argon atmosphere in a tube furnace, followed by drop-quenching in cold water to prevent any decomposition. The specimens were silver-soldered to steel sheets that could be gripped in the micro-tensile device shown in Figure 5. The solution treated specimens were aged at 623 K for various lengths of time in argon atmosphere and quenched in cold water. The specimens were electropolished according to the conditions given in Table 1, and deformed at a constant cross-head speed of 0.05 cm/minute at room temperature using a load of 50 kg. The surfaces of the deformed single crystal specimens were examined by a Hitachi S-415A Scanning Electron Microscope operated at 25 kilovolts.

CHAPTER 3

RESULTS

3.1 Transmission Electron Microscopy of Deformation Structure in Specimens with Large Grains

The details presented in this section are a representative of the results obtained from the analyses of dislocations along potentially operative slip traces in homogenized and aged bulk specimens deformed in uniaxial tension. These analyses were carried out using thin foils which were prepared from these bulk samples. The analyses were aimed at determining the character of these dislocations by identifying the Burgers vector and the corresponding dislocation line direction. The steps used in these analyses are described in the experimental procedure.

In order to determine whether the heat treatment imparted to the Cu-10Ni-6Sn alloy actually causes spinodal decomposition, the electron diffraction patterns of

as-quenched and aged specimens are compared in Figure 14. The sidebands that are visible in the diffraction patterns of the aged specimens clearly indicate that spinodal decomposition did indeed occur by the aging treatments given to the specimens studied in this investigation.

Nineteen representative analyses of dislocation character in specimens that have undergone various extents of spinodal decomposition are provided in this thesis. Dislocations analyzed in homogenized specimens are shown in Figures 15, 16 and 17, in specimens aged for 5 minutes in Figures 18 through 22, in specimens aged for 20 minutes in Figures 23 through 26, in specimens aged for 40 minutes in Figures 27 through 30, and in specimens aged for 60 minutes in Figures 31, 32 and 33. All the aging treatments were carried out at 623 K. In each of these figures bright-field micrographs taken with a different diffraction vector $\vec{g}$, which was determined from the two-beam condition in the diffraction mode are presented. The corresponding diffraction vector and the specimen foil normal are indicated for each micrograph.

It can be noticed from the various micrographs that the dislocations analyzed do not have a unique orientation. Hence the average line direction of the dislocations lying in a single slip trace was considered rather than the specific orientation of individual dislocations. However,

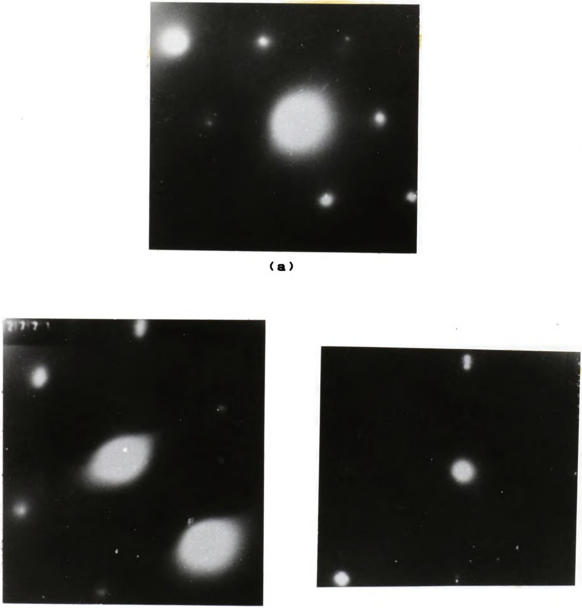

(a)

(b)

(c)

Figure 14: Electron diffraction patterns showing sidebands in specimens aged at 623 K for various lengths of time;

a) as-quenched,

b) aged for 20 minutes at 623 K,

c) aged for 40 minutes at 623 K.

assigning an average direction to a set of dislocations oriented in a random fashion does not have any validity in the absence of faceting. In the present analysis, the average direction was used as a guideline to determine the tendency of the dislocation orientation in the deformation structure.

3.1.1 Homogenized Specimens

Dislocations in two parallel slip traces marked "A" and "A′" are shown in Figure 15. From Figures 15(a) and 15(b), it can be seen that these dislocations (in slip traces "A" and "A′") are in contrast when the operating diffraction vectors are $[\bar{1}1\bar{1}]$ and $[\bar{1}11]$ respectively, and out of contrast when the diffraction vector is $[00\bar{2}]$ (in Figure 15(c)). The Burgers vector analysis of the dislocations is carried out using the accompanying table in which "x" represents that the "$\vec{g}.\vec{b} = 0$" criterion is satisfied and "-" represents that the "$\vec{g}.\vec{b} = 0$" criterion is not satisfied. These notations are used throughout this section.

Figure Number	$\vec{g}$	$\vec{b}$: $[110]$	$[1\bar{1}0]$	$[101]$	$[10\bar{1}]$	$[011]$	$[01\bar{1}]$
15(a)	$[\bar{1}1\bar{1}]$	x	-	-	x	x	-
15(b)	$[\bar{1}11]$	x	-	x	-	-	x
15(c)	$[00\bar{2}]$	x	x	-	-	-	-

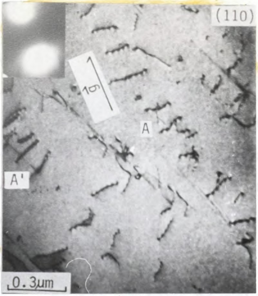

(a)

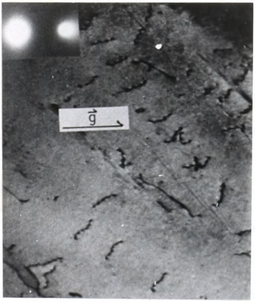

(b)

(c)

Figure 15: Burgers vector analysis of dislocations in slip traces "A" and "A′" in thin foil obtained from homogenized and deformed bulk specimen.

a) $\vec{g} = [\bar{1}1\bar{1}]$

b) $\vec{g} = [\bar{1}11]$ c) $\vec{g} = [00\bar{2}]$

It can be seen from the table that the only possible Burgers vector of the dislocations in slip traces "A" and "A′" is [1$\bar{1}$0]. The dislocation line direction in these slip traces was determined by trace analysis using a standard (110) stereographic projection. The results of this trace analysis are summarized as follows.

Slip Traces	Burgers Vector	Slip System	Average Line Direction	Dislocation Character
A & A′	[1$\bar{1}$0]	(111)[1$\bar{1}$0]	[11$\bar{2}$]	Predominantly Edge
	[1$\bar{1}$0]	(11$\bar{1}$)[1$\bar{1}$0]	[112]	

It can be seen from the analysis that the character of the dislocations in the parallel slip traces "A" and "A′" is predominantly edge.

Dislocations lying along the slip trace marked "B" in Figure 16 are analyzed in another homogenized specimen. These dislocations are in contrast with the $\vec{g}$ vectors being [$\bar{1}$11] and [1$\bar{1}$1] (Figures 16(a) and 16(b) respectively), but out of contrast for a $\vec{g}$ vector of [00$\bar{2}$] (Figure 16(c)). The table for the Burgers vector analysis of these dislocations is shown below.

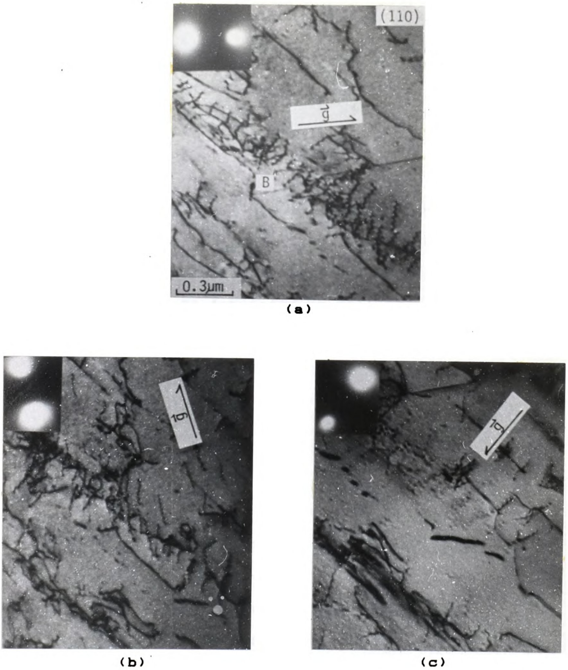

Figure 16: Burgers vector analysis of dislocations in slip trace "B" in thin foil obtained from homogenized and deformed bulk specimen.

a) $\vec{g} = [\bar{1}11]$

b) $\vec{g} = [1\bar{1}1]$

c) $\vec{g} = [00\bar{2}]$

Figure Number	$\vec{g}$	$\vec{b}$ [110]	[1$\bar{1}$0]	[101]	[10$\bar{1}$]	[011]	[01$\bar{1}$]
16(a)	[$\bar{1}$11]	x	-	x	-	-	x
16(b)	[1$\bar{1}$1]	x	-	-	x	x	-
16(c)	[00$\bar{2}$]	x	x	-	-	-	-

The only possible Burgers vector of the dislocations in slip trace "B" is [1$\bar{1}$0]. Results of the trace analysis using a (110) stereographic projection for these dislocations can be tabulated as follows.

Slip Trace	Burgers Vector	Slip System	Average Line Direction	Dislocation Character
B	[1$\bar{1}$0]	(111)[1$\bar{1}$0]	[11$\bar{2}$]	Predominantly Edge
	[1$\bar{1}$0]	(11$\bar{1}$)[1$\bar{1}$0]	[112]	

The results indicate that the character of the dislocations in slip trace "B" is predominantly edge.

Dislocations in two slip traces "C" and "D" shown in Figure 17 are analyzed for their character in a third as-quenched specimen. Dislocations in slip trace "C" are in contrast for $\vec{g}$ vectors [1$\bar{1}$1] and [002], and out of contrast for the $\vec{g}$ vector of [$\bar{1}$11], as shown in Figures 17(a), 17(c) and 17(b) respectively. Dislocations in slip trace "D" are in contrast for $\vec{g}$ = [1$\bar{1}$1] and $\vec{g}$ = [$\bar{1}$11], and out of contrast for $\vec{g}$ = [002], as shown in Figures 17(a), 17(b) and 17(c) respectively.

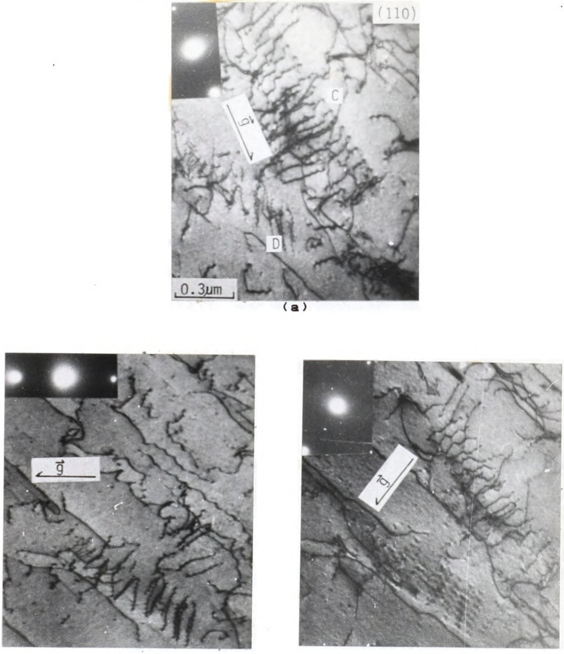

(a)

(b) (c)

Figure 17: Burgers vector analysis of dislocations in slip traces "C" and "D" in thin foil obtained from homogenized and deformed bulk specimen.

a) $\vec{g} = [1\bar{1}1]$

b) $\vec{g} = [\bar{1}11]$ c) $\vec{g} = [002]$

Figure Number	$\vec{g}$	$\vec{b}$ [110]	$[1\bar{1}0]$	[101]	$[10\bar{1}]$	[011]	$[01\bar{1}]$
17(a)	$[1\bar{1}1]$	x	-	-	x	x	-
17(b)	$[\bar{1}11]$	x	-	x	-	-	x
17(c)	[002]	x	x	-	-	-	-

It can be seen from the Burgers vector analysis that the dislocations in slip trace "C" have a Burgers vector of either [101] or $[01\bar{1}]$, and dislocations in slip trace "D" have a Burgers vector of $[1\bar{1}0]$. The results of the trace analysis using a (110) stereographic projection are as follows.

Slip Trace	Burgers Vector	Slip System	Average Line Direction	Dislocation Character
C	[101]	$(11\bar{1})[101]$	[011]	
		$(\bar{1}11)$ - NP		Mixed at about 60° to Burgers vector
	$[01\bar{1}]$	$(111)[01\bar{1}]$	$[10\bar{1}]$	
		$(\bar{1}11)$ - NP		
D	$[1\bar{1}0]$	$(111)[1\bar{1}0]$	$[11\bar{2}]$	Predominantly Edge
	$[1\bar{1}0]$	$(11\bar{1})[1\bar{1}0]$	[112]	

The symbol "NP" in this table and in succeeding tables indicates that the particular slip plane is not a possible slip plane, as indicated by the trace analysis. The analysis from Figure 17 indicated that the dislocations in

slip trace "C" are predominantly mixed whereas those in slip trace "D" are predominantly edge.

3.1.2 Specimens Aged for 5 Minutes

Dislocations observed along the two slip traces marked "E" and "F" in Figure 18 are analyzed for their character in a thin foil prepared from a bulk deformed specimen aged for 5 minutes. These dislocations are seen to be in contrast in Figures 18(a) and 18(c) with diffraction vectors of $[1\bar{1}\bar{1}]$ and $[1\bar{1}1]$ respectively, and they are out of contrast for g = [002] in Figure 18(b). The Burgers vector of these sets of dislocations is determined using the following table:

Figure Number	$\vec{g}$			$\vec{b}$			
		$[110]$	$[1\bar{1}0]$	$[101]$	$[10\bar{1}]$	$[011]$	$[01\bar{1}]$
18(a)	$[1\bar{1}\bar{1}]$	x	-	x	-	-	x
18(b)	$[002]$	x	x	-	-	-	-
18(c)	$[1\bar{1}1]$	x	-	-	x	x	-

The unique Burgers vector of the dislocations in both slip traces "E" and "F" is $[1\bar{1}0]$. Trace analysis using a (110) stereographic projection yields the following results:

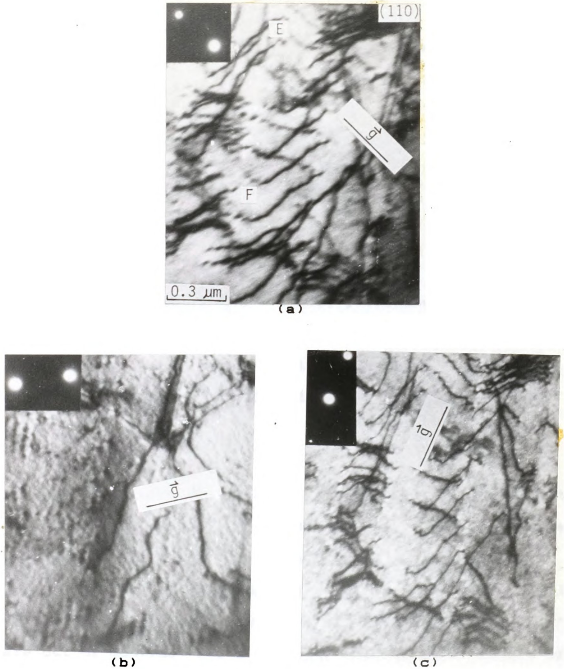

Figure 18: Burgers vector analysis of dislocations in slip traces "E" and "F" in thin foil obtained from aged and deformed bulk specimen. Specimen aged at 623 K for 5 minutes.

a) $\vec{g} = [1\bar{1}\bar{1}]$

b) $\vec{g} = [002]$ c) $\vec{g} = [1\bar{1}1]$

Slip Trace	Burgers Vector	Slip System	Average Line Direction	Dislocation Character
E	$[1\bar{1}0]$	$(111)[1\bar{1}0]$	$[10\bar{1}]$	Mixed predominantly at 60° to Burgers vector
	$[1\bar{1}0]$	$(11\bar{1})[1\bar{1}0]$	$[011]$	
F	$[1\bar{1}0]$	$(111)[1\bar{1}0]$	$[01\bar{1}]$	Mixed predominantly at 60° to Burgers vector
	$[1\bar{1}0]$	$(11\bar{1})[1\bar{1}0]$	$[101]$	

Dislocations in slip traces "E" and "F" are analyzed to be of mixed character and oriented predominantly at 60 degrees to their Burgers vector. It is apparent that these dislocations are lying on parallel slip planes but are oriented along two <110> directions at 60 degrees to each other.

Burgers vector analysis of dislocations is carried out for the dislocations in a second specimen along slip traces "G" and "H" in Figure 19. Dislocations in slip trace "G" are in contrast in both Figures 19(a) and 19(b) ($\vec{g} = [\bar{1}11]$ and $\vec{g} = [1\bar{1}1]$ respectively), whereas those in slip trace "H" are out of contrast for $\vec{g} = [1\bar{1}1]$. The Burgers vectors of the dislocations in slip traces "G" and "H" are analyzed as follows.

Figure Number	$\vec{g}$	$\vec{b}$: $[110]$	$[1\bar{1}0]$	$[101]$	$[10\bar{1}]$	$[011]$	$[01\bar{1}]$
19(a)	$[\bar{1}11]$	x	-	-	x	x	-
19(b)	$[1\bar{1}1]$	x	-	x	-	-	x

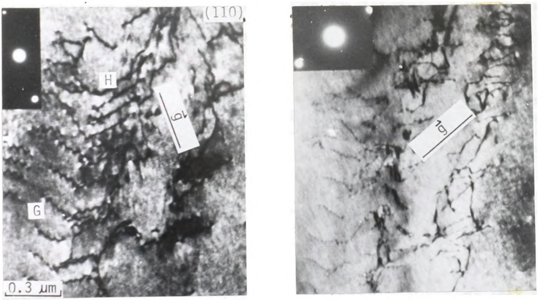

(a) (b)

Figure 19: Burgers vector analysis of dislocations in slip traces "G" and "H" in thin foil obtained from aged and deformed bulk specimen. Specimen aged at 623 K for 5 minutes.

a) $\vec{g} = [\bar{1}11]$ b) $\vec{g} = [1\bar{1}1]$

The obvious Burgers vector of the dislocations in slip trace "G" is $[1\bar{1}0]$, whereas that of the dislocations in slip trace "H" is either $[10\bar{1}]$ or $[011]$. The character of the dislocations in these slip traces is determined using trace analysis with a (110) stereographic projection.

Slip Trace	Burgers Vector	Slip System	Average Line Direction	Dislocation Character
G	$[1\bar{1}0]$	$(111)[1\bar{1}0]$	$[11\bar{2}]$	Predominantly Edge
	$[1\bar{1}0]$	$(11\bar{1})[1\bar{1}0]$	$[112]$	
H	$[10\bar{1}]$	$(111)[1\bar{1}0]$	$[01\bar{1}]$	
		$(1\bar{1}1)$ - NP		Mixed predominantly at 60° to Burgers vector
	$[011]$	$(11\bar{1})[1\bar{1}0]$	$[101]$	
		$(\bar{1}\bar{1}1)$ - NP		

It can be seen that the dislocations in slip trace "G" are predominantly of the edge character, whereas those in slip trace "H" are mixed and oriented predominantly at 60 degrees to their Burgers vector.

Dislocations in a third specimen aged for 5 minutes lying along the slip trace "J" are seen to be in contrast for diffraction vectors $[\bar{1}11]$ and $[1\bar{1}1]$ in Figures 20(a) and 20(b) respectively. The following table is used to determine the Burgers vector.

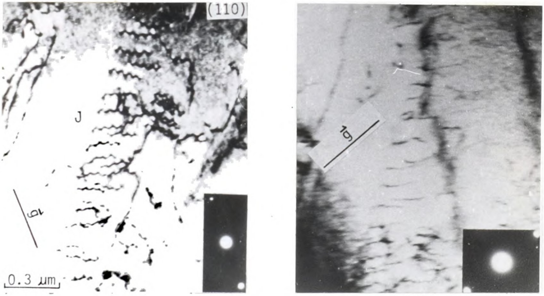

(a) (b)

Figure 20: Burgers vector analysis of dislocations in slip trace "J" in thin foil obtained from aged and deformed bulk specimen. Specimen aged at 623 K for 5 minutes.

a) $\vec{g} = [\bar{1}11]$ b) $\vec{g} = [1\bar{1}1]$

Figure Number	$\vec{g}$	$\vec{b}$ [110]	[1$\bar{1}$0]	[101]	[10$\bar{1}$]	[011]	[01$\bar{1}$]
20(a)	[$\bar{1}$11]	x	-	-	x	x	-
20(b)	[1$\bar{1}$1]	x	-	x	-	-	x

Since the dislocations are in contrast in both of the micrographs, the obvious Burgers vector of these dislocations is [1$\bar{1}$0]. Trace analysis to determine the dislocation character using a (110) stereographic projection yields the following results:

Slip Trace	Burgers Vector	Slip System	Average Line Direction	Dislocation Character
J	[1$\bar{1}$0]	(111)[1$\bar{1}$0]	[11$\bar{2}$]	Predominantly Edge
	[1$\bar{1}$0]	(11$\bar{1}$)[1$\bar{1}$0]	[112]	

The analysis carried out above indicates that the dislocations in slip trace "J" are predominantly edge.

Dislocations lying along the slip trace "K" in Figure 21 are analyzed for their character. They are present in a fourth specimen aged for 5 minutes. These dislocations are in contrast in Figures 21(a) ($\vec{g}$ = [1$\bar{1}\bar{1}$]) and 21(c) ($\vec{g}$ = [00$\bar{2}$]) but are out of contrast in Figure 21(b) ($\vec{g}$ = [1$\bar{1}$1]).

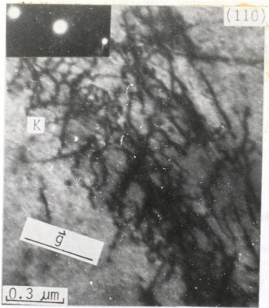

(a)

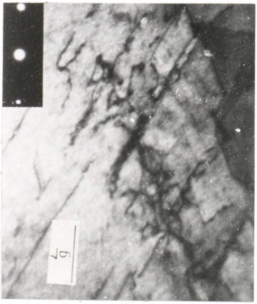

(b)

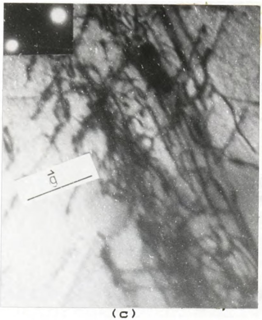

(c)

Figure 21: Burgers vector analysis of dislocations in slip trace "K" in thin foil obtained from aged and deformed bulk specimen. Specimen aged at 623 K for 5 minutes.

a) $\vec{g} = [1\bar{1}\bar{1}]$

b) $\vec{g} = [1\bar{1}1]$ c) $\vec{g} = [00\bar{2}]$

Figure Number	$\vec{g}$	$\vec{b}$ [110]	$[1\bar{1}0]$	[101]	$[10\bar{1}]$	[011]	$[01\bar{1}]$
21(a)	$[1\bar{1}\bar{1}]$	x	-	x	-	-	x
21(b)	$[1\bar{1}1]$	x	-	-	x	x	-
21(c)	$[00\bar{2}]$	x	x	-	-	-	-

From the table outlined above, the Burgers vector of the dislocations in slip trace "K" is determined to be either $[10\bar{1}]$ or [011]. Trace analysis is employed with the aid of a (110) stereographic projection and the dislocation character of the dislocations in slip trace "K" is determined.

Slip Trace	Burgers Vector	Slip System	Average Line Direction	Dislocation Character
K	$[10\bar{1}]$	$(111)[1\bar{1}0]$	$[01\bar{1}]$	
		$(1\bar{1}1)$ - NP		Mixed at about 60° to Burgers vector
	[011]	$(11\bar{1})[1\bar{1}0]$	[101]	
		$(1\bar{1}1)$ - NP		

The analyses indicate that the dislocations along slip trace "K" are predominantly mixed, being oriented at about 60 degrees to their Burgers vector.

Dislocations along the slip trace "L" (in Figure 22) are analyzed in a yet another specimen aged for 5 minutes. Since these dislocations are in contrast for both $\vec{g} = [1\bar{1}\bar{1}]$ (Figure 22(a)) and for $\vec{g}$ = [002] (Figure 22(b)), their

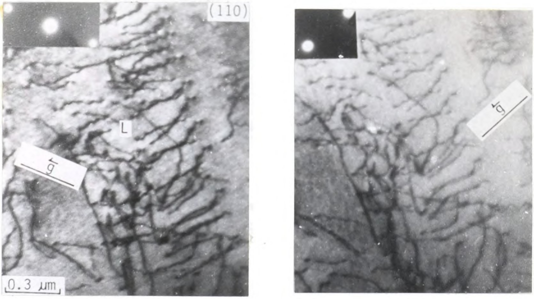

(a) (b)

Figure 22: Burgers vector analysis of dislocations in slip trace "L" in thin foil obtained from aged and deformed bulk specimen. Specimen aged at 623 K for 5 minutes.

a) $\vec{g} = [1\bar{1}\bar{1}]$ b) $\vec{g} = [002]$

Burgers vector is either $[10\bar{1}]$ or $[011]$, as determined from the following table:

Figure Number	$\vec{g}$	$\vec{b}$ $[110]$	$[1\bar{1}0]$	$[101]$	$[10\bar{1}]$	$[011]$	$[01\bar{1}]$
22(a)	$[1\bar{1}\bar{1}]$	x	-	x	-	-	x
22(b)	$[002]$	x	x	-	-	-	-

Trace analysis using a (110) stereographic projection yields the following results:

Slip Trace	Burgers Vector	Slip System	Average Line Direction	Dislocation Character
L	$[10\bar{1}]$	$(111)[1\bar{1}0]$	$[01\bar{1}]$	
		$(1\bar{1}1)$ - NP		Mixed at about 60° to Burgers vector
	$[011]$	$(11\bar{1})[110]$	$[101]$	
		$(1\bar{1}1)$ - NP		

The analysis above indicates that the dislocations in slip trace "L" are mixed and tend to be oriented at 60 degrees to their Burgers vector.

3.1.3 Specimens Aged for 20 Minutes

Dislocations lying along the slip trace marked "M" in Figure 23 have been analyzed in a foil prepared from a specimen aged at 623 K for 20 minutes. The apparent direction of motion of the dislocations is indicated by the

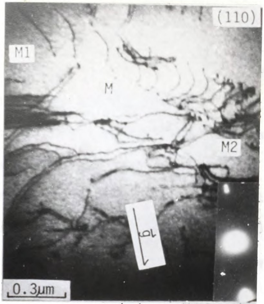

(a)

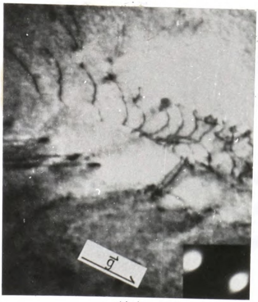

(b)

(c)

Figure 23: Burgers vector analysis of dislocations in slip trace "M" in thin foil obtained from aged and deformed bulk specimen. Specimen aged at 623 K for 20 minutes.

a) $\vec{g} = [002]$

b) $\vec{g} = [\bar{1}1\bar{1}]$

c) $\vec{g} = [1\bar{1}\bar{1}]$

arrow in Figure 23(a), which is deduced from the shape of the dislocation lines. The most interesting feature in this analysis is that the dislocations near the region marked "M1" have an entirely different character as compared to the dislocations near the region marked "M2". It can be seen that all these dislocations are in contrast for $\vec{g}$ = [002] (Figure 23(a)) and $\vec{g}$ = $[\bar{1}1\bar{1}]$ (Figure 23(b)), but out of contrast for $\vec{g}$ = $[1\bar{1}\bar{1}]$ (Figure 23(c)). The Burgers vector is determined using the following table.

Figure Number	$\vec{g}$	$\vec{b}$: [110]	$[1\bar{1}0]$	[101]	$[10\bar{1}]$	[011]	$[01\bar{1}]$
23(a)	[002]	x	x	-	-	-	-
23(b)	$[\bar{1}1\bar{1}]$	x	-	-	x	x	-
23(c)	$[1\bar{1}\bar{1}]$	x	-	x	-	-	x

It can be seen that dislocation in slip trace "M" have a Burgers vector of either [101] or $[01\bar{1}]$. Trace analysis using a (110) stereographic projection yields the following results:

Slip Trace	Burgers Vector	Slip System	Average Line Direction	Dislocation Character
M1	[101]	$(11\bar{1})[101]$	[101]	
		$(\bar{1}11)$ - NP		Predominantly Screw
	$[01\bar{1}]$	$(111)[01\bar{1}]$	$[01\bar{1}]$	
		$(\bar{1}11)$ - NP		
M2	[101]	$(11\bar{1})[101]$	$[\bar{1}10]$	
		$(\bar{1}11)$ - NP		Mixed at about 60° to Burgers vector
	[011]	$(111)[01\bar{1}]$	$[\bar{1}10]$	
		$(\bar{1}11)$ - NP		

It is apparent from these findings that the dislocations have reoriented from a screw character at the top left corner of the micrographs (near M1) to a mixed character at about 60 degrees to their Burgers vector at the bottom right corner of the micrographs (near M2) during their progression along the slip trace "M".

Dislocations lying along the slip trace marked "N" in Figure 24 in a second specimen aged for 20 minutes are in contrast for $\vec{g} = [00\bar{2}]$ and $\vec{g} = [1\bar{1}\bar{1}]$ (Figures 24(a) and 24(b) respectively) and out of contrast for $\vec{g} = [\bar{1}1\bar{1}]$ (Figure 24(c)). The Burgers vector of the dislocations in slip trace "N" is determined from the following table:

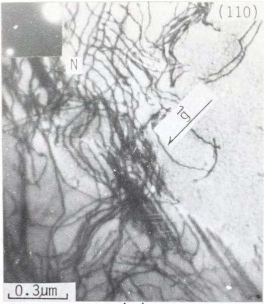

(a)

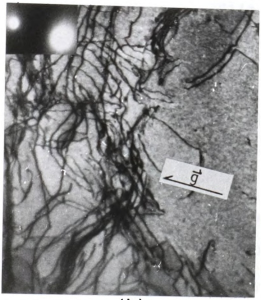

(b)

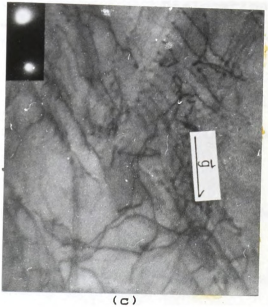

(c)

Figure 24: Burgers vector analysis of dislocations in slip trace "N" in thin foil obtained from aged and deformed bulk specimen. Specimen aged at 623 K for 20 minutes.

a) $\vec{g} = [00\bar{2}]$

b) $\vec{g} = [1\bar{1}\bar{1}]$ c) $\vec{g} = [\bar{1}1\bar{1}]$

Figure Number	$\vec{g}$	$\vec{b}$ [110]	$[1\bar{1}0]$	[101]	$[10\bar{1}]$	[011]	$[01\bar{1}]$
24(a)	$[00\bar{2}]$	x	x	-	-	-	-
24(b)	$[1\bar{1}\bar{1}]$	x	-	x	-	-	x
24(c)	$[\bar{1}1\bar{1}]$	x	-	-	x	x	-

The results indicate that the dislocations in slip trace "N" have a Burgers vector of either $[10\bar{1}]$ or [011]. Trace analysis using a (110) stereographic projection yields the following results:

Slip Trace	Burgers Vector	Slip System	Average Line Direction	Dislocation Character
N	$[10\bar{1}]$	$(111)[01\bar{1}]$	$[1\bar{1}0]$	Mixed predominantly at 60° to Burgers vector
		$(1\bar{1}1)$ - NP		
	[011]	$(11\bar{1})[101]$	$[1\bar{1}0]$	
		$(1\bar{1}1)$ - NP		

The Burgers vector and trace analysis indicate that the dislocations present in the slip trace "N" are of mixed character and predominantly oriented at 60 degrees to their Burgers vector.

Dislocations lying along the slip trace marked "P" in a third specimen aged for 20 minutes are shown in Figure 25. These dislocations are in contrast for the $[1\bar{1}\bar{1}]$ and $[00\bar{2}]$ diffraction vectors and out of contrast for the $[\bar{1}1\bar{1}]$ diffraction vector, as shown in Figures 25(a), 25(b) and

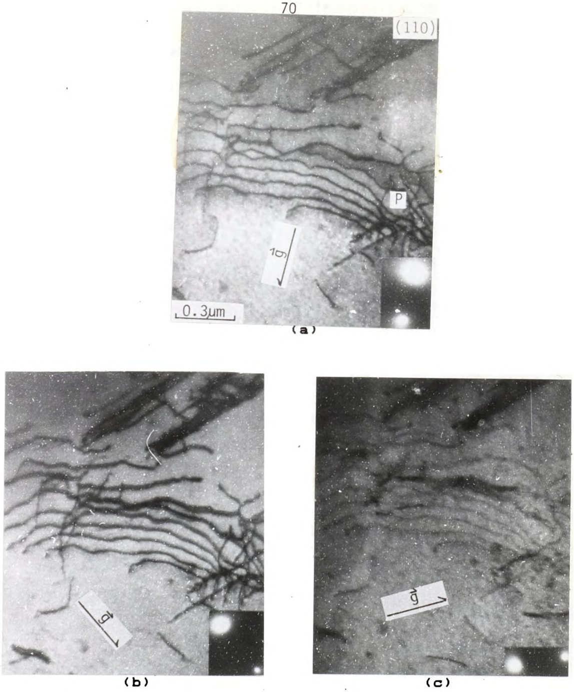

Figure 25: Burgers vector analysis of dislocations in slip trace "P" in thin foil obtained from aged and deformed bulk specimen. Specimen aged at 623 K for 20 minutes.

a) $\vec{g} = [1\bar{1}\bar{1}]$

b) $\vec{g} = [00\bar{2}]$

c) $\vec{g} = [\bar{1}1\bar{1}]$

25(c) respectively. The table for determining the Burgers vector of the dislocations in slip trace "P" is shown below.

Figure Number	$\vec{g}$	$\vec{b}$ [110]	$[1\bar{1}0]$	[101]	$[10\bar{1}]$	[011]	$[01\bar{1}]$
25(a)	$[1\bar{1}\bar{1}]$	x	-	x	-	-	x
25(b)	$[00\bar{2}]$	x	x	-	-	-	-
25(c)	$[\bar{1}1\bar{1}]$	x	-	-	x	x	-

The results indicate that the Burgers vector of the dislocations in slip trace "P" is either $[10\bar{1}]$ or [011]. Trace analysis using a (110) stereographic projection gives the following results:

Slip Trace	Burgers Vector	Slip System	Average Line Direction	Dislocation Character
P	$[10\bar{1}]$	$(111)[10\bar{1}]$	$[01\bar{1}]$	
		$(1\bar{1}1)$ - NP		Mixed predominantly at 60° to Burgers vector
	[011]	$(11\bar{1})[011]$	[101]	
		$(1\bar{1}1)$ - NP		

The analyses indicate that the dislocations in slip trace "P" are predominantly of mixed character.

Dislocations along the slip trace "Q" in Figure 26 are analyzed for their character in yet another specimen aged for 20 minutes. In Figure 26(a), these dislocations are in

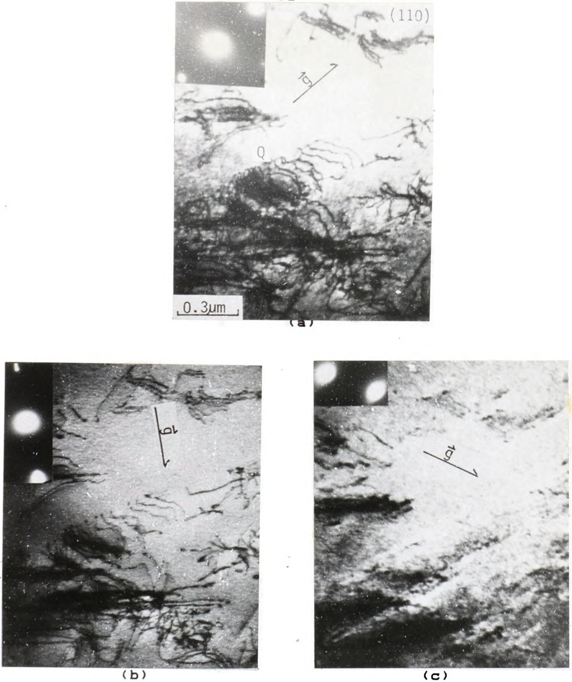

Figure 26: Burgers vector analysis of dislocations in slip trace "Q" in thin foil obtained from aged and deformed bulk specimen. Specimen aged at 623 K for 20 minutes.

a) $\vec{g} = [1\bar{1}\bar{1}]$

b) $\vec{g} = [002]$ c) $\vec{g} = [\bar{1}1\bar{1}]$

contrast for a diffraction vector of $[\bar{1}\bar{1}1]$, they are once again in contrast for g = [002] in Figure 26(b), but they are out of contrast for g = $[\bar{1}1\bar{1}]$ in Figure 26(c). The Burgers vector of these dislocations is determined using the following table:

Figure Number	$\vec{g}$	$\vec{b}$ [110]	$[1\bar{1}0]$	[101]	$[10\bar{1}]$	[011]	$[01\bar{1}]$
26(a)	$[\bar{1}\bar{1}1]$	x	-	x	-	-	x
26(b)	[002]	x	x	-	-	-	-
26(c)	$[\bar{1}1\bar{1}]$	x	-	-	x	x	-

The dislocations in slip trace "Q" have a Burgers vector of either $[10\bar{1}]$ or [011], and their character is determined from the following trace analysis using a (110) stereographic projection.

Slip Trace	Burgers Vector	Slip System	Average Line Direction	Dislocation Character
Q	$[10\bar{1}]$	$(111)[10\bar{1}]$	$[01\bar{1}]$	
		$(1\bar{1}1)$ - NP		Mixed at about 60° to Burgers vector
	[011]	$(11\bar{1})[011]$	[101]	
		$(1\bar{1}1)$ - NP		

The analysis of dislocations in slip trace "Q" indicates that they are of mixed character oriented at about 60 degrees to their Burgers vector.

3.1.4 Specimens Aged for 40 Minutes

Dislocations lying along the slip trace marked "R" in a foil prepared from a specimen aged for 40 minutes at 623 K are shown in Figure 27. It can be observed that these dislocations are in contrast for $\vec{g}$ = [$\bar{1}$11] (Figure 27(a)) and for $\vec{g}$ = [002] (Figure 27(b)), but out of contrast for $\vec{g}$ = [$\bar{1}1\bar{1}$] (Figure 27(c)). The Burgers vector of these dislocations is determined from the following table:

Figure Number	$\vec{g}$	$\vec{b}$ [110]	[1$\bar{1}$0]	[101]	[10$\bar{1}$]	[011]	[01$\bar{1}$]
27(a)	[$\bar{1}$11]	x	-	x	-	-	x
27(b)	[002]	x	x	-	-	-	-
27(c)	[$\bar{1}1\bar{1}$]	x	-	-	x	x	-

The Burgers vector of the dislocations in slip trace "R" is either [10$\bar{1}$] or [011]. The trace analysis using a (110) stereographic projection for determining the character of these dislocations yields the following results:

Slip Trace	Burgers Vector	Slip System	Average Line Direction	Dislocation Character
R	[10$\bar{1}$]	(111)[01$\bar{1}$]	[10$\bar{1}$]	
		(1$\bar{1}$1) - NP		Predominantly Screw
	[011]	(11$\bar{1}$)[101]	[011]	
		(1$\bar{1}$1) - NP		

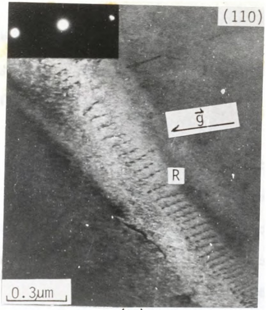

(a)

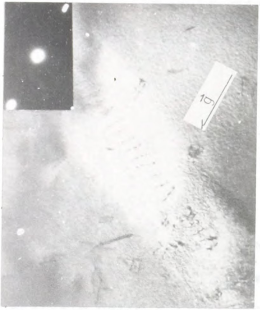

(b)

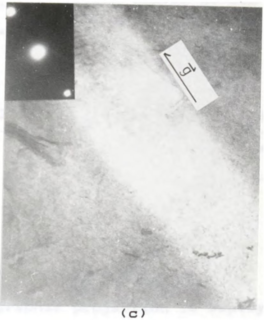

(c)

Figure 27: Burgers vector analysis of dislocations in slip trace "R" in thin foil obtained from aged and deformed bulk specimen. Specimen aged at 623 K for 40 minutes.

a) $\vec{g} = [\bar{1}11]$

b) $\vec{g} = [002]$ c) $\vec{g} = [\bar{1}1\bar{1}]$

The analysis of dislocations lying along slip trace "R" in a specimen aged for 40 minutes indicates that they are predominantly of screw character.

Analysis of dislocation character for the dislocations present in slip trace "S" in Figure 28 is shown for a second specimen aged for 40 minutes. These dislocations can be observed to be in contrast for a diffraction vector of $\vec{g}$ = $[\bar{1}11]$ in Figure 28(a) and out of contrast for a diffraction vector of $\vec{g}$ = [002] in Figure 28(b). The following table is used for the identification of the Burgers vector of the dislocations in slip trace "S".

Figure Number	$\vec{g}$	$\vec{b}$ [110]	$[1\bar{1}0]$	[101]	$[10\bar{1}]$	[011]	$[01\bar{1}]$
28(a)	$[\bar{1}11]$	x	-	x	-	-	x
28(b)	[002]	x	x	-	-	-	-

The Burgers vector can be seen to be $[1\bar{1}0]$ for the dislocations in slip trace "S". The following trace analysis using a (110) stereographic projection is employed to determine the character of these dislocations.

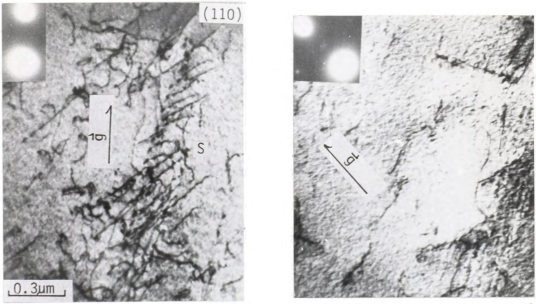

(a) (b)

Figure 28: Burgers vector analysis of dislocations in slip trace "S" in thin foil obtained from aged and deformed bulk specimen. Specimen aged at 623 K for 40 minutes.

a) $\vec{g}$ = $[\bar{1}11]$, b) $\vec{g}$ = [002]

Slip Trace	Burgers Vector	Slip System	Average Line Direction	Dislocation Character
S	$[1\bar{1}0]$	$(111)[1\bar{1}0]$	$[01\bar{1}]$	Mixed predominantly at 60° to Burgers vector
	$[1\bar{1}0]$	$(11\bar{1})[1\bar{1}0]$	$[101]$	

The dislocations along slip trace "S" are seen to be of mixed character and oriented predominantly at 60 degrees to their Burgers vector.

Dislocations lying along parallel slip traces "T" and "T′" in Figure 29 are analyzed for their character in a third specimen aged for 40 minutes. All these dislocations are in contrast for diffraction vectors $[\bar{2}20]$ and $[020]$, as seen in Figures 29(a) and 29(b) respectively. They are out of contrast when the diffraction vector is $[220]$, as seen in Figure 29(c). The Burgers vector for these dislocations is determined using the following table:

Figure Number	$\vec{g}$			$\vec{b}$			
		$[110]$	$[1\bar{1}0]$	$[101]$	$[10\bar{1}]$	$[011]$	$[01\bar{1}]$
29(a)	$[\bar{2}20]$	x	-	-	-	-	-
29(b)	$[020]$	x	-	x	x	-	-
29(c)	$[220]$	x	x	-	-	-	-

The unique Burgers vector of these dislocations is $[1\bar{1}0]$. The characters of the different dislocations are determined by trace analysis using a (100) stereographic

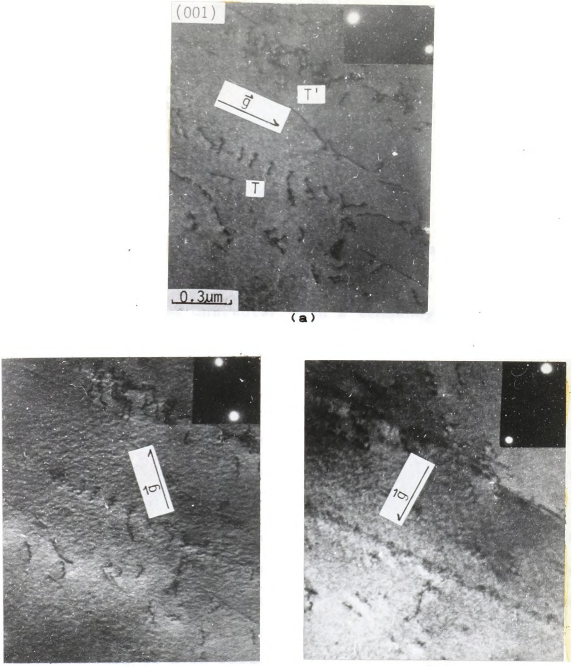

(a)

(b) (c)

Figure 29: Burgers vector analysis of dislocations in slip traces "T" and "T′" in thin foil obtained from aged and deformed bulk specimen. Specimen aged at 623 K for 40 minutes.

a) $\vec{g} = [\bar{2}20]$

b) $\vec{g} = [020]$ c) $\vec{g} = [220]$

projection.

Slip Traces	Burgers Vector	Slip System	Average Line Direction	Dislocation Character
T & T′	$[1\bar{1}0]$	$(111)[1\bar{1}0]$	$[0\bar{1}1]$	Mixed at about 60° to Burgers vector
	$[1\bar{1}0]$	$(11\bar{1})[1\bar{1}0]$	$[011]$	

The Burgers vector and trace analysis of the dislocations along slip traces "T" and "T′" indicate that they are of mixed character with a tendency to be oriented at 60 degrees to their Burgers vector.

Figure 30 illustrates bright-field micrographs of parallel dislocations present along the slip trace marked "U" in a fourth specimen aged for 40 minutes. Diffracting conditions with g = $[1\bar{1}\bar{1}]$ and g = [002], where the dislocations are in contrast, and with g = $[\bar{1}1\bar{1}]$, where the dislocations are out of contrast are shown in Figures 30(a), 30(b) and 30(c) respectively. The following table is used for the determination of the Burgers vector of the dislocations in slip trace "U".

Figure Number	$\vec{g}$	$\vec{b}$ [110]	$[1\bar{1}0]$	[101]	$[10\bar{1}]$	[011]	$[01\bar{1}]$
30(a)	$[1\bar{1}\bar{1}]$	x	-	x	-	-	x
30(b)	[002]	x	x	-	-	-	-
30(c)	$[\bar{1}1\bar{1}]$	x	-	-	x	x	-

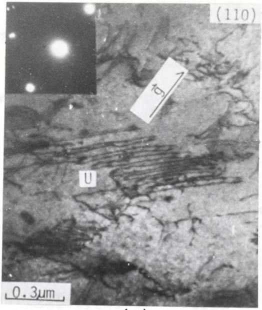

(a)

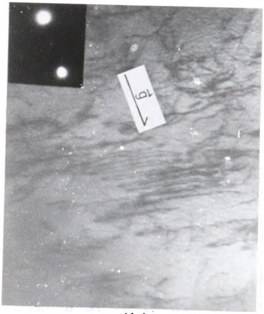

(b)

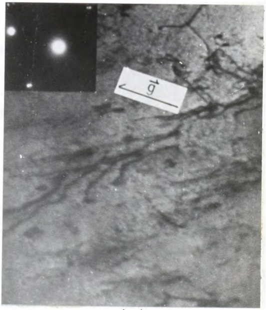

(c)

Figure 30: Burgers vector analysis of dislocations in slip trace "U" in thin foil obtained from aged and deformed bulk specimen. Specimen aged at 623 K for 40 minutes.

a) $\vec{g} = [1\bar{1}\bar{1}]$

b) $\vec{g} = [002]$ c) $\vec{g} = [\bar{1}1\bar{1}]$

Dislocations in slip trace "U" have a Burgers vector of either $[10\bar{1}]$ or $[011]$. The character of the dislocations is identified by trace analysis using a (110) stereographic projection.

Slip Trace	Burgers Vector	Slip System	Average Line Direction	Dislocation Character
U	$[10\bar{1}]$	$(111)[01\bar{1}]$	$[1\bar{1}0]$	
		$(1\bar{1}1)$ - NP		Mixed predominantly at 60° to Burgers vector
	$[011]$	$(11\bar{1})[101]$	$[1\bar{1}0]$	
		$(1\bar{1}1)$ - NP		

The Burgers vector and trace analysis indicate that the dislocations in slip trace "U" are of mixed character and oriented predominantly at 60 degrees to their Burgers vector.

3.1.5 Specimens Aged for 60 Minutes

Dislocations present along the slip trace marked "V"in Figure 31 in a thin foil prepared from a deformed sample aged for 60 minutes are analyzed. These dislocations are in contrast for $\vec{g} = [1\bar{1}1]$ in Figure 31(a), in contrast for $\vec{g} = [002]$ in Figure 31(b), and out of contrast for $\vec{g} = [1\bar{1}\bar{1}]$ in Figure 31(c). The Burgers vector of these dislocations is identified using the following table:

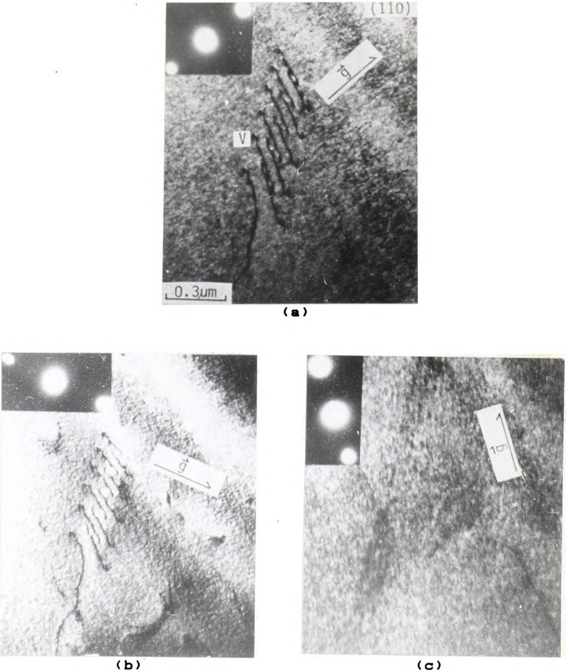

Figure 31: Burgers vector analysis of dislocations in slip trace "V" in thin foil obtained from aged and deformed bulk specimen. Specimen aged at 623 K for 60 minutes.

a) $\vec{g} = [1\bar{1}1]$

b) $\vec{g} = [002]$ c) $\vec{g} = [1\bar{1}\bar{1}]$

Figure Number	$\vec{g}$	$\vec{b}$ [110]	$[1\bar{1}0]$	[101]	$[10\bar{1}]$	[011]	$[01\bar{1}]$
31(a)	$[1\bar{1}1]$	x	-	-	x	x	-
31(b)	[002]	x	x	-	-	-	-
31(c)	$[1\bar{1}\bar{1}]$	x	-	x	-	-	x

It can be seen from the analysis that the dislocations in slip trace "V" have a Burgers vector of either [101] or $[01\bar{1}]$. Trace analysis using a (110) stereographic projection is employed to identify the character of these dislocations.

Slip Trace	Burgers Vector	Slip System	Average Line Direction	Dislocation Character
V	[101]	$(11\bar{1})[1\bar{1}0]$	[011]	Mixed at 60° to Burgers vector
		$(\bar{1}11)$ - NP		
	$[01\bar{1}]$	$(111)[1\bar{1}0]$	$[10\bar{1}]$	
		$(\bar{1}11)$ - NP		

The results indicate that the character of the dislocations present in slip trace "V" is mixed as these dislocations are oriented at 60 degrees to their Burgers vector.

Bright-field micrographs of dislocations in the slip trace "W" are illustrated in Figure 32 in a second specimen aged for 60 minutes. These dislocations are in contrast when the diffraction vector is $[\bar{1}11]$ (Figure 32(a)) and out

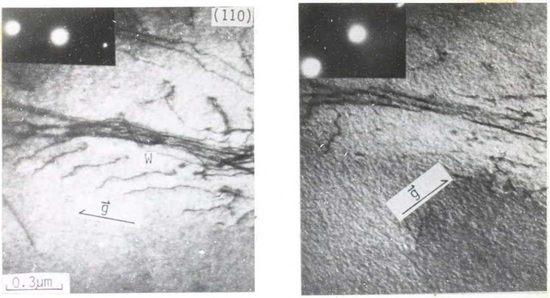

(a) (b)

Figure 32: Burgers vector analysis of dislocations in slip trace "W" in thin foil obtained from aged and deformed bulk specimen. Specimen aged at 623 K for 60 minutes.

a) $\vec{g} = [\bar{1}11]$ b) $\vec{g} = [002]$

of contrast when the diffraction vector is [002] (Figure 32(b)). The Burgers vector of the dislocations in slip trace "W" is determined as follows.

Figure Number	$\vec{g}$	$\vec{b}$ [110]	$[1\bar{1}0]$	[101]	$[10\bar{1}]$	[011]	$[01\bar{1}]$
32(a)	$[\bar{1}11]$	x	-	x	-	-	x
32(b)	[002]	x	x	-	-	-	-

Since the dislocations are out of contrast for $\vec{g}$ = [002], it is apparent that their Burgers vector is $[1\bar{1}0]$. The character of these dislocations is determined by trace analysis using a (110) stereographic projection, as shown by the following table.

Slip Trace	Burgers Vector	Slip System	Average Line Direction	Dislocation Character
W	$[1\bar{1}0]$	$(111)[1\bar{1}0]$	$[10\bar{1}]$	Mixed predominantly at 60° to Burgers vector
	$[1\bar{1}0]$	$(11\bar{1})[1\bar{1}0]$	[011]	

The analysis of dislocations in Figure 31 indicates that the dislocations in slip trace "W" are mixed, lying predominantly at 60 degrees to their Burgers vector.

Analysis of dislocation character for the dislocations present in parallel slip traces "X", "X′" and "X″" in Figure 33 is carried out in a third specimen aged for 60 minutes.

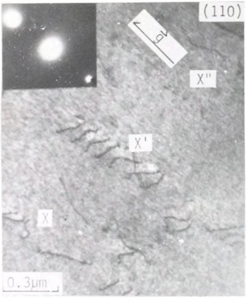

(a)

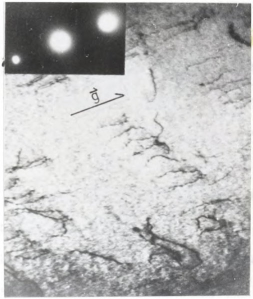

(b)

Figure 33: Burgers vector analysis of dislocations in slip traces "X", "X'" and "X"" in thin foil obtained from aged and deformed bulk specimen. Specimen aged at 623 K for 60 minutes.

a) $\vec{g} = [\bar{1}1\bar{1}]$ b) $\vec{g} = [1\bar{1}\bar{1}]$

These dislocations are in contrast when the diffraction vector is $[\bar{1}1\bar{1}]$ as well as when it is $[1\bar{1}\bar{1}]$, as shown in Figures 33(a) and 33(b) respectively. The Burgers vector of the dislocations in slip traces "X", "X′" and "X″" is determined as follows.

Figure Number	$\vec{g}$	$\vec{b}$ $[110]$	$[1\bar{1}0]$	$[101]$	$[10\bar{1}]$	$[011]$	$[01\bar{1}]$
33(a)	$[\bar{1}1\bar{1}]$	x	-	-	x	x	-
33(b)	$[1\bar{1}\bar{1}]$	x	-	x	-	-	x

Since the dislocations are in contrast in both Figures 33(a) and 33(b), it is apparent that the only possible Burgers vector of the dislocations is $[1\bar{1}0]$. Trace analysis using a (110) stereographic projection is employed to identify the dislocation character.

Slip Traces	Burgers Vector	Slip System	Average Line Direction	Dislocation Character
X, X′ &	$[1\bar{1}0]$	$(111)[01\bar{1}]$	$[10\bar{1}]$	Mixed at about 60° to Burgers vector
X″	$[1\bar{1}0]$	$(11\bar{1})[101]$	$[011]$	

Once again the analysis indicates that the dislocations present in the slip traces "X", "X′" and "X″" in the specimen aged for 60 minutes are mixed, and tend to be oriented at 60 degrees to their Burgers vector.

Results of the dislocation character analyses for the

different specimens are summarized in Table 3.

3.2 Single Crystal Specimens

Plastic deformation of all the single crystal specimens deformed in uniaxial tension along the $[\bar{1}45]$ tensile axis started as single slip in the mid-section of the specimens. It was noticed that single slip propagated along the length of the specimens until it reached the regions near the silver-soldered ends of the specimens. Slip distribution in specimens that have undergone 5% elongation is shown in the scanning electron micrographs of Figure 34. It can be noticed from this figure that the homogenized specimen deformed by relatively finer slip as compared to the aged specimens.

Further deformation of all the single crystal specimens was observed to occur by extensive single slip, and the entire plastic deformation of all the specimens was confined to Stage I of the stress-strain curve. Extensive single slip of homogenized and aged single crystal specimens is observed in regions away from the fracture surface as shown in the micrographs in Figure 35.

The maximum stress level reached in each specimen was found to cause severe localized plastic deformation. This localized deformation occurred near the region where

Table 3 Summary of Dislocation Character Analyses in Specimens Aged at 623 K and Deformed in Bulk.

Aging Time (Minutes)	Figure Number	Slip Trace	Predominant Character
0	15	A	Edge
		A	Edge
0	16	B	Edge
0	17	C	Mixed
		D	Edge
5	18	E	Mixed
		F	Mixed
5	19	G	Edge
		H	Mixed
5	20	J	Edge
5	21	K	Mixed
5	22	L	Mixed
20	23	M1	Screw
		M2	Mixed
20	24	N	Mixed
20	25	P	Mixed
20	26	Q	Mixed
40	27	R	Screw
40	28	S	Mixed
40	29	T	Mixed
		T	Mixed
40	30	U	Mixed
60	31	V	Mixed
60	32	W	Mixed
60	33	X	Mixed
		X	Mixed
		X"	Mixed

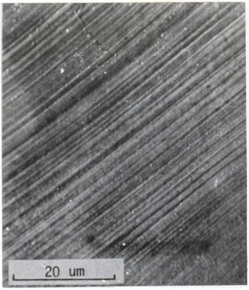

(a)

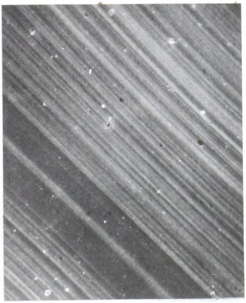

(b)

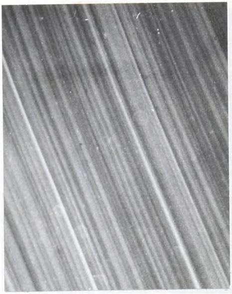

(c)

Figure 34: Slip traces in single crystal specimens at 5% plastic strain;

a) homogenized.

b) aged at 623 K for 20 minutes.

c) aged at 623 K for 240 minutes.

(a)

(b)

(c)

Figure 35: Slip traces in single crystal specimens in regions away from the fracture surface;

a) homogenized.

b) aged at 623 K for 20 minutes.

c) aged at 623 K for 240 minutes.

fracture took place ultimately and was found to consist of multiple slip. Intersecting slip observed in the severely deformed regions near the fracture surface is illustrated in the micrographs shown in Figure 36. All the specimens deformed in a ductile manner, and the typical ductile fracture surface is shown in a specimen aged at 623 K for 240 minutes in Figure 37.

Quantitative data from the deformation studies on the single crystal specimens are presented in Table 4. It can be seen that the critical resolved shear stress increases with increasing aging time but parameters such as the work-hardening rate and the total elongation are not affected by the extent of spinodal decomposition. The plots of engineering stress versus engineering strain are provided for two cases, one at very early stages and the other at later stages of spinodal decomposition, in Figure 38.

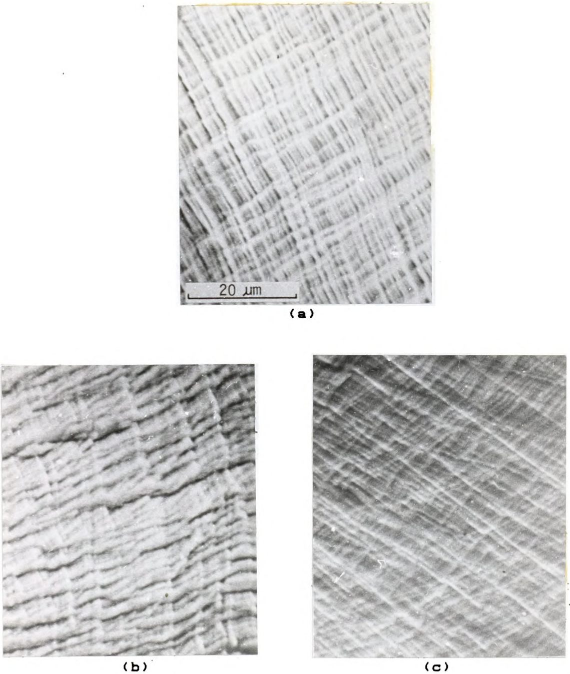

Figure 36: Slip distribution in regions of single crystal specimens that have undergone severe localized plastic deformation (near fracture).

a) homogenized.

b) aged at 623 K for 20 minutes.

c) aged at 623 K for 240 minutes.

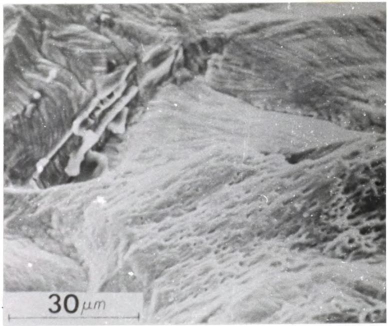

Figure 37: Ductile fracture surface in a single crystal specimen aged at 623 K for 240 minutes.

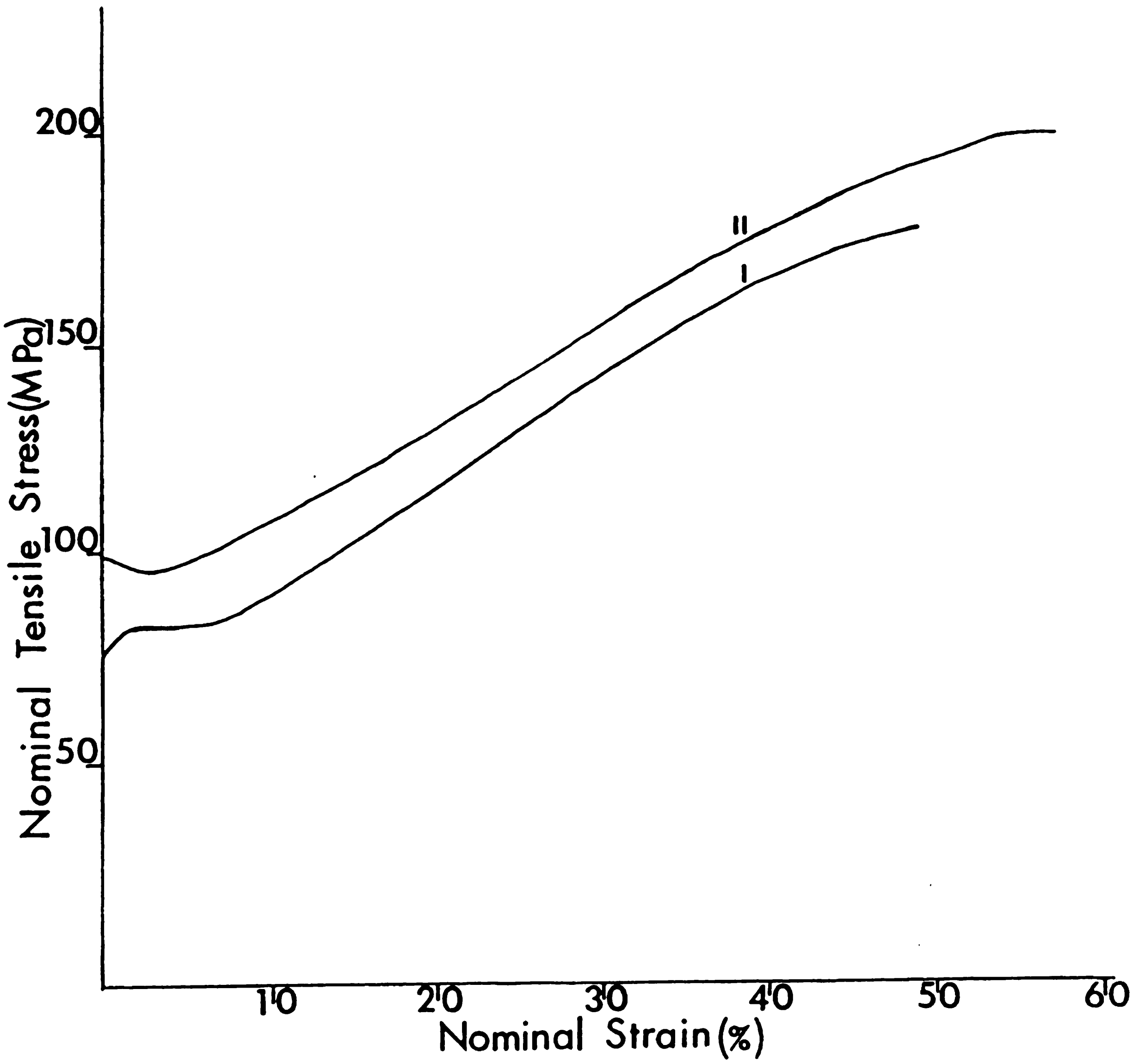

Figure 38: Nominal tensile stress versus nominal strain plot for single crystal specimens aged at 623 K for different lengths of time (I - 5 minutes, II - 240 minutes).

Table 4 Tensile Test Data for Single Crystal Specimens Aged at 623 K.

Aging Time (Min.)	Critical Resolved Shear Stress (MPA)	Work-Hardening Rate (MPA/unit strain)	Total Elongation (%)
0	35.34	267	48.0
5	38.07	275	49.3
20	40.42	256	53.8
240	46.06	240	57.0

CHAPTER 4

DISCUSSION

4.1 Transmission Electron Microscopy of Large-Grained Specimens

Plastic flow in a crystalline material occurs as a result of the motion of dislocations, so that mechanical properties like the strength and ductility of a crystal are determined by the behavior of dislocations. The materials science approach has been developed so far on the basis of the theory of dislocations.

The major aim of this study has been to analyze the character of dislocations responsible for the deformation in deformed bulk specimens of the Cu-10Ni-6Sn spinodal alloy in order to experimentally verify which of the various proposed theories can successfully explain the age-hardening mechanism in spinodal alloys. This is necessary as all the acceptable theories [10, 20, 22] are based on a specific

character of the dislocations.

4.1.1 Merits and Demerits of Comparative Studies

In the early stages of deformation, slip in face-centered cubic alloys appears to proceed by co-operative glide, that is, by the movement of large dislocation groups. The resultant structure can be seen in the transmission electron micrographs of foils prepared from the specimens that have undergone the earlier stages of deformation in bulk as a group of more or less parallel dislocations with the same Burgers vector. Dislocation loops emanating from sources (like Frank-Read sources) are rarely seen in their entirety during transmission electron microscopic studies, unless the thin section is cut more or less parallel to an active slip plane. Under normal conditions, the active slip plane will be inclined to the foil surface and as a result only a part of the dislocation line can be observed. Based on this limited information, the overall dislocation behavior during deformation is interpreted.

An explanation of the results presented in the previous section is provided in this chapter. In analyzing the character of the dislocations lying along slip traces in foils prepared from specimens deformed in bulk, it is assumed that these have been responsible for the

macroyielding of the bulk specimens. Whether the dislocations concerned had indeed been responsible for the macroyielding of the specimens cannot be fully ascertained by such a method. Therefore the results obtained in this study are compared to those obtained by <u>in-situ</u> deformation studies on thin foil specimens of the same alloy in the High Voltage Electron Microscope (HVEM) [46].

The major advantage of <u>in-situ</u> straining studies is that the behavior of the dislocations can be observed during deformation. Besides, use of the HVEM for such studies can facilitate observation on thicker foils that may be more representative of bulk specimens. In order that the results obtained are representative of that in bulk specimens, specimens of thicknesses of a few micrometers (depending on the atomic number of the major constituents) are necessary [47]. However, this condition necessitates ultra-high voltage electron microscopes for effective electron penetration of the thick foils, which can cause extensive radiation damage within a short period [46, 48]. It can be seen that these two phenomena imply contradictory voltage conditions.

Preparation of foils that are of uniform thickness for TEM observations is impossible except by vapor deposition. However, preparation of alloy specimens, and their handling for <u>in-situ</u> straining, make the specimen preparation by

vapor deposition unsuitable. Electrochemically thinned specimens for in-situ straining invariably will have varying thickness in the electron-transparent regions. As a result, the exact state and the magnitude of the stress in thin regions due to an applied uniaxial loading cannot be obtained. In addition, due to this complicated state of stress, one cannot be certain whether the first mobile dislocations in the region of observation had indeed been responsible for the macroyielding phenomenon.

4.1.2 Analysis of Results from Comparative Studies

4.1.2 (i) Homogenized Specimens

In the case of face-centered cubic alloys, under an applied stress, screw components of a dislocation loop have been observed to move farther than the edge components, resulting in loops elongated in the direction perpendicular to the Burgers vector [50-54]. This is attributed to the friction due to the lattice on edge dislocations exceeding that on screw dislocations. The operation of a Frank-Read source under such conditions will be controlled by overcoming the lattice friction on edge dislocations [51-53]. In addition, the process of thinning the deformed bulk specimen for TEM studies can alter the dislocation configurations to some extent [55]. A prime example of such a phenomenon is that the screw components of the dislocation

loops frequently tend to move out of the foil due to their higher mobility, leaving predominantly the edge components behind [55]. Hence the probability of observing edge dislocations along slip traces of foils prepared from deformed homogenized bulk specimens is much higher than screw dislocations. Results of the analyses of dislocations in potentially operative slip traces of homogenized specimens shown in Figures 15, 16 and 17 are consistent with the above observations.

On the contrary, screw dislocations were consistently observed in the deformation structure obtained during the <u>in-situ</u> deformation of thin foils of homogenized specimens of the same alloy [46]. This contradiction can be explained on the following basis. The regions observed in the <u>in-situ</u> deformation experiments were below the critical thickness required to represent the behavior of bulk specimens [51], and hence the dislocation multiplication by the activation of Frank-Read sources was not possible [56, 57]. In such thin specimens of face-centered cubic alloys, the multiplication of dislocations results from surface dislocation sources of the screw type [58, 59]. It has also been reported that <u>in-situ</u> deformation techniques on specimens with sub-critical thickness cause dislocations which face the higher resistance from the lattice to escape through the surfaces; those dislocations which face the lower resistance propagate along the slip traces [58, 59].

Since the lattice friction on edges exceeds that on screws in face-centered cubic alloys, the dislocations that were mobile during <u>in-situ</u> straining of homogenized thin foils tended to exist in screw orientation in their relaxed configuration under stress.

4.1.2 (ii) Specimens Aged at 623 K for Shorter Periods of Time

Dislocations analyzed along slip traces that had been potentially operative in specimens aged for 5 and 20 minutes indicated that most of the dislocations were predominantly of mixed character with varying orientations. In specimens aged for 5 minutes, dislocations of predominantly edge character were observed in a few slip traces as well. In Figure 18, the dislocations present in slip traces "E" and "F" are mixed in character. If an average direction can be assigned to these two sets of dislocations, it would be approximately 60 degrees to their common Burgers vector, namely, [110]. These two sets of dislocations are apparently of opposite signs. However, assigning an average direction to a set of dislocations oriented in a random fashion does not have any validity in the absence of dislocation faceting. In the present analysis, the average direction was used as a guideline to determine the tendency of the dislocation orientation in the deformation structure. Dislocations in slip trace "H" in Figure 19, "K" in Figure

21 and "L" in FIgure 22 are of mixed character as well, whereas those in slip traces "G" and "J" in Figure 20 are predominantly edge.

The analysis of dislocations along potentially active slip traces of specimens aged for 20 minutes at 623 K and deformed in bulk indicated that all these dislocations were predominantly mixed. Once again, if an average orientation was assigned to the dislocations in these slip traces, it would be about 60 degrees to their Burgers vector. As has been pointed out earlier, this is used only as a guideline to determine the tendency of the dislocation orientation in the deformation structure, since there was no dislocation faceting. In Figure 23, analysis of the dislocations along the slip trace "M" indicated that part of the dislocations are screw while the others are predominantly mixed. From the shape of the dislocation lines (the curvature) it is apparent that these dislocations have progressed from the region marked "M1" towards the region marked "M2" during the tensile deformation of the bulk specimen. This observation suggests that the screw dislocations may have reoriented into the mixed character during their motion in this aged specimen. In Figures 24, 25 and 26 the dislocations along the potentially operative slip traces are all predominantly mixed.

In an ideally modulated face-centered cubic spinodal

alloy mixed dislocations oriented at 60 degrees to their Burgers vector have the lowest energy configuration among all orientations [60]. In addition, dislocations possessing this configuration face the maximum resistance due to the internal stress field and, during their motion under an applied stress, the dislocation segments tend to orient into a configuration predominantly at 60 degrees to their Burgers vector. Therefore, in an ideally modulated microstructure, dislocations that are responsible for the yielding should either exist in this particular configuration or should reorient into this character during the intial stages of plastic deformation. However, during transmission electron microscopic analysis of dislocations present in potentially active slip traces of spinodally modulated specimens deformed in bulk, effects due to the modulation and its inhomogeneities, effects due to the solid solution and its local inhomogeneities, as well as effects due to the thin foil preparation have to be taken into consideration. In specimens aged for shorter periods (say, 5 minutes) the effect of modulation is apparently not dominant enough to overcome the role of the other factors. Under such conditions, the solid-solution hardening effect may still be important as evidenced by the presence of dislocations of predominantly edge character in the deformation structure of some of the specimens.

In addition to the effects already mentioned, the

significant role of the surface has to be taken into account while considering results based on _in-situ_ straining of thin foils. In specimens that have undergone the earlier stages of spinodal decomposition (upto 20 minutes aging at 623 K) the modulation effects are not strong enough to overcome the surface effects. As a result, dislocations that were mobile during _in-situ_ straining tend to exist in screw orientation in their relaxed configuration under stress, just as in the case of homogenized specimens.

4.1.2 (iii) Specimens Aged at 623 K for Longer Periods of Time

Burgers vector analysis of dislocations present in foils prepared from deformed bulk specimens aged for 40 minutes indicates that mixed dislocations may be responsible for the deformation in these specimens. These dislocations are shown in Figures 27 through 30. Similar mixed dislocations were very consistently observed in slip traces of specimens aged for 60 minutes. These mixed dislocations can be seen in the micrographs presented in Figures 31, 32 and 33. These mixed dislocations were more or less predominantly oriented at 60 degrees to their respective Burgers vector.

It is evident that the effect due to the composition modulation resulting from longer aging times is dominant enough to effectively overcome the other factors mentioned

earlier. Hence the dislocations tended to reorient into a configuration in which they experience the maximum resistance to their motion from the internal stress field. These results are in good agreement with those obtained from in-situ deformation studies of specimens that were aged for longer periods of time, namely, 60 minutes. In such specimens, in spite of the surface effects, the dislocations that were mobile during straining were observed to exist in a mixed orientation at 60 degrees to their Burgers vector in their equilibrium congiguration under stress.

The results based on this present study indicate that the dislocations responsible for deformation do not acquire any specific character in specimens that have undergone earlier stages of spinodal decomposition. However, there is a tendency for the dislocations to reach the specific configuration assumed in the model proposed by Kato et al. [20]. This apparent difference can be attributed to the existence of non-ideal microstructure in real materials, unlike the one considered in the model. In real materials that have undergone extensive aging, effects due to the composition modulation are dominant enough for the dislocations to reach the specific mixed character that would exist in an ideally modulated microstructure. Such an explanation is consistent with the results obtained from the two parallel studies (TEM of deformed bulk specimens and

in-situ straining of thin foils in HVEM [46]).

4.2 Single Crystal Specimens

4.2.1 Critical Resolved Shear Stress

Comparison of the values of critical resolved shear stress of Cu-Ni-Sn single crystal specimens aged at 623 K for various lengths of time and oriented for single slip indicates that increased time of aging (or increased extent of spinodal decomposition) causes increases in the critical resolved shear stress. This hardening may be attributed to the coherency internal stress field resulting from early stages of spinodal decomposition. However, this observed incremental critical resolved shear stress is only about one-half of the corresponding incremental yield stress values of polycrystalline specimens that had undergone similar aging heat treatments [38], assuming a Taylor factor of 3 for converting polycrystalline yield stress to critical resolved shear stress. The Taylor theory [61] is based on deriving the shear stress-shear strain curve for polycrystalline specimens from the shear stress-shear strain curve for a single crystal oriented for single slip, considering the compatibility of deformations in the different grains in order to assure intergranular cohesion.

4.2.2 Work-Hardening Rate

It can be noticed from the data in Table 4 that the work-hardening rate is apparently independent of the extent of spinodal decomposition with an average value of about 260 MPa/unit strain for specimens aged upto 4 hours at 623 K. This observation is in good agreement with those on polycrystalline specimens of the same alloy [37, 38]. A possible explanation for this apparent independence of the work-hardening rate on the extent of composition modulation is that the impediment for dislocation motion due to the diffuse obstacles present in the modulated structure, once overcome by the applied stress, is not dominant enough to cause dislocation pile-ups that can result in an increase in the work-hardening rates. Evidences obtained during <u>in-situ</u> deformation studies on large-grained specimens of the same alloy in the HVEM distinctly support such an explanation [46]. The leading dislocation in the slip trace marked "ST" in Figure 39(a) was observed to move in an extremely discontinuous manner, with alternating periods of rest and motion. It is evident that the barrier provided by the diffuse obstacles was responsible for hindering the motion of the leading dislocations. However, effects due to increasing amounts of deformation and the pile-up stress of the trailing dislocations cause the leading dislocations to overcome the barrier and proceed further along the slip

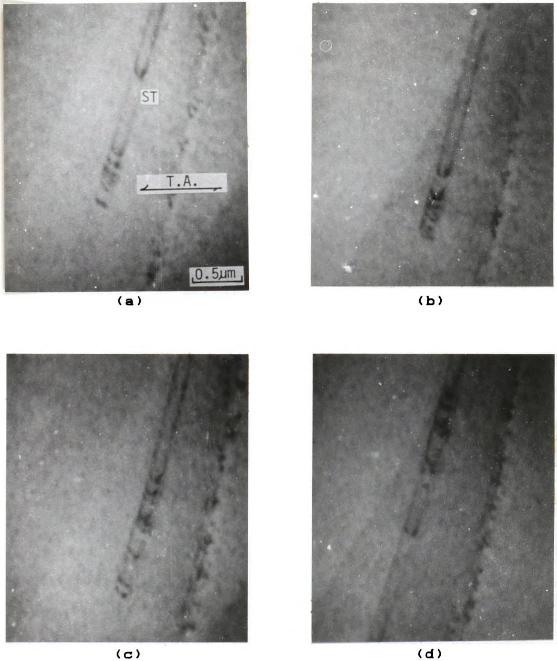

Figure 39: Series of micrographs showing the motion of dislocations along the slip trace marked "ST" in an aged specimen deformed *in-situ* in the High Voltage Electron Microscope [46]. Specimen aged at 623 K for 40 minutes.

trace, as evidenced in Figures 39 (b), (c) and (d). It is clear from the set of micrographs that the barrier to dislocation motion caused by the modulated structure is not effective enough to create a dislocation pile-up that could have subsequently led to an increase in the work-hardening rate.

4.2.3 Total Elongation

The extent of spinodal decomposition does not apparently affect the ductility of the different single crystal specimens of this alloy oriented for single slip. This is clearly illustrated by an average value of about 50% plastic strain for fracture in the various specimens, as shown in Table 4. This phenomenon can be explained on the following basis. Dislocations activated by the external applied stress are apparently able to move through the pseudo-particles resulting from the composition modulation with relative ease in aged specimens, although apparently with more difficulty as compared to the dislocations in homogenized specimens. The diffuse obstacles in the modulated structure do not act as strong enough barriers to the glide motion of dislocations. The motion of dislocations through a spinodally modulated matrix during <u>in-situ</u> deformation in the HVEM shown in Figure 39 further supports this viewpoint. Stronger obstacles could cause a pile-up of dislocations and the resultant nucleation of cracks, leading to lower ductility in specimens that have undergone extensive aging, where precipitation or second phase particles can result.

4.2.4 Slip Distribution in Deformed Specimens

It can be seen from the scanning electron micrographs in Figure 34 that the homogenized single crystal specimens have relatively finer slip bands as compared to the aged specimens. According to Quin and Schwartz [41, 42], the motion of the first dislocations along a slip trace in an aged specimen tends to demodulate that particular slip trace, leading to localized decreases in the coherency strains. the slip traces where dislocation motion has taken place initially in aged specimens thus become energetically more favorable for subsequent dislocation motion. The tendency for dislocation motion to be concentrated on particular slip traces leads to the formation of relatively coarse slip bands. Large-grained specimens with a modulated structure, during in-situ deformation in the HVEM, tend to deform by the motion of dislocations in closely spaced parallel slip planes. This feature is clearly illustrated in Figure 40 in a specimen aged for 40 minutes at 623 K, where the co-ordinated motion of dislocations can be seen in the closely spaced parallel slip planes "B", "C" and "D". An explanation for co-ordinated slip in aged specimens may be provided as follows. The stress created by the pseudo

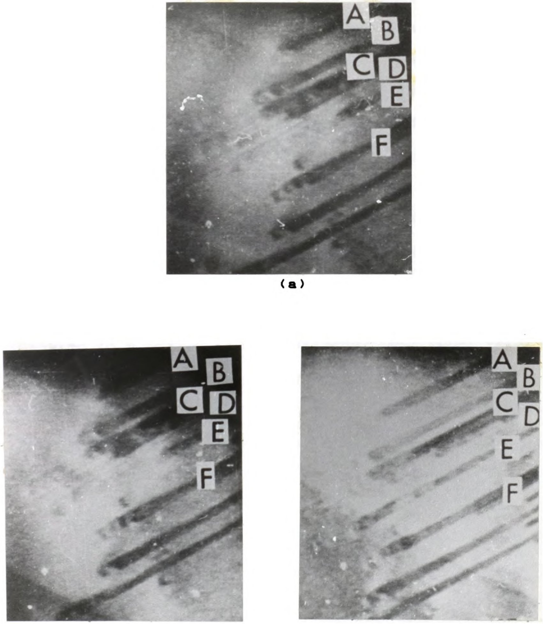

(a)

(b)

(c)

Figure 40: Co-ordinated slip observed in an aged specimen during in-situ deformation in the High Voltage Electron Microscope. Specimen aged at 623 K for 40 minutes.

pile up of dislocations due to the diffuse obstacles in the modulated structure could cause the motion of dislocations in closely spaced adjacent slip traces, leading to co-ordinated slip. Such co-ordinated slip observed in aged specimens during electron microscopic studies may account for the coarse slip observed in them in optical and scanning electron microscopy of deformed specimens. In the case of the homogenized matrix, the slip traces where dislocation motion takes place initially are not energitically any more favorable than the other slip traces, hence dislocation motion can occur simultaneously in more slip traces as compared to a modulated matrix. This phenomenon leads to relatively finer slip bands as compared to the aged specimens. These results are fully consistent with the observations in polycrystalline specimens of the same alloy [38].

CHAPTER 5

CONCLUSIONS

1. Dislocations present in potentially active slip traces of homogenized specimens of Cu-10Ni-6Sn alloy were found to be predominantly of edge character, which is consistent with models suggesting that edge components of dislocation loops face the highest resistance to their motion in face-centered cubic solid solutions.

2. Dislocations possessing fairly random orientations were observed in slip traces of specimens that had undergone the earlier stages of spinodal decomposition (upto 20 minutes aging at 623 K), although there was a tendency for these dislocations to be oriented at 60 degrees to their Burgers vector. The difference in dislocation character, as compared to that in homogenized specimens, can be attributed to the modulated structure created by spinodal decomposition.

3. Dislocations present in slip traces of specimens that had undergone extensive composition modulation (more than 40 minutes aging at 623 K) were predominantly oriented at 60 degrees to their Burgers vector, which is apparently due to the dominant effects of the composition modulation.

4. The results obtained during the present study seem to favor the theory of Kato, Mori and Schwartz [20], for an ideally modulated structure, among the various theories. However, in real materials, local inhomogeneities in the matrix and in the composition modulation play significant roles and have to be taken into consideration in models dealing with age-hardening during earlier stages of spinodal decomposition.

5. The entire deformation of homogenized and aged single crystal specimens oriented for single slip took place in Stage I.

6. The ductility and work-hardening rate of the single crystal specimens are independent of the extent of spinodal decomposition. These findings are in good agreement with those in polycrystalline specimens of the same alloy [38].

7. The slip bands observed in the homogenized specimens are

relatively fine as compared to those in the aged specimens. These observations are also consistent with those on polycrystalline specimens of the same alloy [38].

REFERENCES

1. Cahn, J. W., "Spinodal Decomposition", Trans. AIME, 242, 166 (1968).

2. Nicholson, R. B. and Tufton, P. J., "Precipitation Procedures of Hard Magnetic Materials", Z. Angew Physik, 2, 59 (1966).

3. Gibbs, J. W., Collected Works (New Haven, Yale University Press, 1948) p. 105 and 252.

4. Hillert, M., "A Solid-Solution Model for Inhomogeneous System", Acta Metall., 9, 525 (1961).

5. Hilliard, J. E. and Cahn, J. W., "Free Energy of a Non-Uniform System", J. Chem. Phys., 28, 258 (1958).

6. Cahn, J. W., "On Spinodal Decomposition", Acta Metall., 9, 795 (1961).

7. Bradley, A. J., cited in Reference 8.

8. Daniel, V. and Lipson, H., "An X-ray Study of the Dissociation of an Alloy of Copper, Iron and Nickel", Proceedings of the Royal Society (London), Serial A, 181, 368 (1943).

9. Daniel, V. and Lipson, H., Proceedings of the Royal Society (London), Serial A, 182, 378 (1944).

10. Cahn, J. W., "Hardening by Spinodal Decomposition", Acta Metall., 11, 1275 (1963).

11. Douglass, D. L. and Barbee, T. W., "Spinodal Decomposition in Al/Zn Alloys", J. Mater. Sci., 4, 121 (1969).

12. Ditchek, B. and Schwartz, L. H., "Application of Spinodal Alloys", Annual Review of Materials Science, 9, 219 (1979).

13. Lefevre, B. G., D'Annessa, A. T. and Kalish, D., "Age Hardening in Cu-15Ni-8Sn Alloy", Met. Trans., 9A, 577 (1978).

14. Butler, E. P. and Thomas, G., "Structure and Properties of Spinodally Decomposed Cu-Ni-Fe Alloys", Acta Metall., 18, 347 (1970).

15. Carpenter, R. W., "Deformation and Fracture of Gold-Platinum Polycrystals Strengthened by Spinodal Decomposition", Acta Metall., 15, 1297 (1967).

16. Ditchek, B. and Schwartz, L. H., Proceeding of the 4th International Conference on Strength of Metals and Alloys, 3, 1319 (1976).

17. Ghista, D. N. and Nix, W. D., "A Dislocation Model Pertaining to the Strength of Elastically Inhomogeneous Materials", Mat. Sci. and Eng., 3, 293 (1969).

18. Dahlgren, S. D., "Dislocation Interactions with Internal Coherency Stress in Age-Hardened Cu-Ni-Fe Alloys", Met. Trans., 7A, 1661 (1976).

19. Hanai, Y., Miyazaki, T. and Mori, H., "Theoretical Estimation of the Effect of Interfacial Energy on the Mechanical Strength of Spinodally Decomposed Alloys", J. Mater. Sci., 14, 599 (1979).

20. Kato, M., Mori, T. and Schwartz, L. H., "Hardening by Spinodal Modulated Structure", Acta Metall., 28, 285 (1980).

21. Wagner, R., cited in Reference 22.

22. Ardell, A. J., "Precipitation Hardening", Met. Trans. A, in press.

23. Mott, N. F., Imperfections in Nearly Perfect Crystals, Shockley, W., Hollomon, J. H., Maurer, R. and Seitz, F. eds., John Wiley & Sons, New York, NY, 1952, p.173.

24. Nabarro, F. R. N., "The Statistical Problem of Hardening", J. Less-Common Metals, 28, 257 (1972).

25. Schwartz, L. H., Mahajan, S. and Plewes, J. T., "Spinodal Decomposition in a Cu-9Ni-6Sn Alloy", Acta Metall., 22, 601 (1974).

26. Livak, R. J. and Thomas, G., "Spinodally Decomposed Cu-Ni-Fe Alloys of Asymmetrical Compositions", Acta Metall., 19, 497 (1971).

27. Laughlin, D. E., "Spinodal Decomposition in Nickel Based Ni-Ti Alloys", Acta Metall., 24, 53, (1976).

28. Ditchek, B. and Schwartz, L. H., "Diffraction Study of Spinodal Decomposition in Cu-10Ni-6Sn", Acta Metall., 28, 807 (1980).

29. Wu, C. K. and Thomas, G., "Microstructure and Properties of a Cu-Ni-Cr Alloy", Met. Trans., 8A, 1911 (1977).

30. Dahlgren, S. D., "Correlation of Yield Strength with Internal Coherency Stress in Age-Hardened Cu-Ni-Fe Alloys", Met. Trans., 8A, 347 (1977).

31. Chou, A., Datta, A., Meier, G. H. and Soffa, W. A., "Microstructure Behaviour and Mechanical Hardening in a Cu-Ni-Sn Alloy", J. Mater. Sci., 13, 541 (1978).

32. Datta, A. and Soffa, W. A., "The Structure and Properties of Age Hardened Cu-Ti Alloys", Acta Metall., 24, 987 (1976).

33. Wagner, R., "Hardening by Modulated Structures in Cu-Ti Alloys", Proceeding of the 5th International Conference on Strength of Metals and Alloys, Aachen, 1979, Haasen P. ed., (Pergamon, Toronto, 1980), p. 645.

34. Laughlin, D. E. and Cahn, J. W., "Spinodal Decomposition in Age Hardened Copper-Titanium alloys", Acta Metall., 23, 329 (1975).

35. Greggi, J. and Soffa, W. A., "Preliminary Observations of the Flow and Fracture of Copper-Titanium Alloy Single Crystals Containing Coherent Precipitates", Scripta Metall., 12, 525 (1978).

36. Kratochvil, P. and Haasen, P., "A Model for an Anomaly in the Age Hardening of Cu-Ti Single Crystals", Scripta Metall., 16, 179 (1982).

37. Kato, M. and Schwartz, L. H., "The Temperature Dependence of Yield Stress and Work Hardening in Spinodally Decomposed Cu-10Ni-6Sn Alloy", Mat. Sci. and Eng., 41, 137 (1979).

38. Vilassakdanont, A. and Subramanian, K. N., "Effect of Temperature on Some of the Mechanical Properties of Cu-10Ni-6Sn Spinodal Alloy", Phys. Stat. Sol., 88, 553 (1985).

39. Lee, T. C., Shekhar, S., Vilassakdanont, A and Subramanian, K. N., "Mechanical Properties of Cu-10Ni-6Sn Alloy", Phase Transformation in Solids, Materials Research Society Symposia Proceedings, Tsakalakos, T. ed., North-Holland Publisher (1984), p. 577.

40. Shekhar, S., Lee, T. C. and Subramanian, K. N., "Deformation Studies of Cu-Ni-Sn Spinodal Alloy", Phys. Stat. Sol., in press.

41. Quin, M. P. and Schwartz, L. H., "Low Cycle Fatigue in Spinodal Cu-10Ni-6Sn", Mat. Sci. and Eng., 46, 249 (1980).

42. Quin, M. P. and Schwartz, L. H., "High Cycle Fatigue Behavior of Spinodal Cu-10Ni-6Sn", Mat. Sci. and Eng., 54, 121 (1982).

43. Louzon, T. J., "Tensile Property Improvements of Spinodal Cu-15Ni-8Sn by Two-Phase Heat Treatment", Trans. ASME, 104, 234 (1982).

44. Schwartz, L. H. and Plewes, J. T., "Spinodal Decomposition in Cu-9Ni-6Sn - II. A Critical Examination of Mechanical Strength of the Spinodal Alloys", Acta Metall., 22, 911 (1974).

45. Sinning, H. -R. and Haasen, P., "The Fatigue Behaviour of Spinodally Decomposed Cu-4Ti Single Crystals", Scripta Metall., 15, 85 (1981).

46. Lee, T. C., Ph. D. Thesis, Michigan State University, 1985.

47. Fujita, H., Kawasaki, Y. and Furubayashi, E., "Metallurgical Investigations with a 500KV Electron Microscope", Japan. J. appl. Phys., 6, 214 (1967)

48. Martin, J. L. and Kubin, L. P., "Optimum Conditions for Straining Experiments in HVEM", Phys. Stat. Sol. 56, 487 (1979).

49. Neuhäuser, H., "Slip-Line Formation and Collective Dislocation Motion", Dislocations in Solids, Nabarro, F. R. N. ed., North-Holland Publishing Company, Vol. 6, 1983, p.321.

50. Neuhäuser, H., Koropp, J. and Heege, R., "Electron Microscopic Studies in the Yield Region of 70/30-α-Brass Single Crystals - I. The Mode of Slip", Acta Metall., 23, 441 (1975).

51. Kleintges, M., "Multiplication of Dislocations in Copper 0.6At% Aluminum Single Crystals", Scripta Metall., C14, 93 (1980).

52. Kleintges, M. and Haasen, P., "Revised Measurements of Dislocation Velocities in Cu-Al Single Crystals", Scripta Metall., 14, 999 (1980).

53. Friedrichs, J. and Haasen, P., "Mobility of Dislocations in Copper-Aluminum Single Crystals", Z. Metallk., 72, 102 (1981).

54. Prinz, F., Karnthaler, H. P. and Kirchner, H. O. K.,"A Study of the Anisotropy of the Friction Stress in Cu-Al Alloys" Acta Metall., 29, 1029 (1981).

55. Honeycombe, R. W. K., The Plastic Deformation of Metals, Edward Arnold (Publishers) Limited, London, 1984, p.52.

56. Fujita, H., "In-Situ Deformation by High Voltage Electron Microscopy", Electron Microscopy, Sturgess, J. M., ed., Ninth International Congress on Electron Microscopy, 3, 355 (1978).

57. Kubin, L. P., Louchet, F. Caillard, D. and Martin, J. L., "Dislocation Multiplication by HVEM In-Situ Straining Experiments", Electron Microscopy, 4, 288 (1980).

58. Vesely, D., "In-Situ Deformation of Molybdenum Thin Foils", J. Microscopy, 97, 191 (1973).

59. Vesely, D., "The Study of Deformation of Thin Foils of Mo Under the Electron Microscope", Phys. Stat. Sol., 29, 675 (1968).

60. Kato, M., Mori, T. and Schwartz, L. H., "The Energetics of Dislocation Motion in Spinodally Modulated Structures", Mat. Sci. and Eng., 51, 25 (1981).

61. Taylor, G. I., J. Inst. Metals, 62, 307 (1938).